



Published in final edited form as:

Neuron. 2022 August 17; 110(16): 2625–2645.e7. doi:10.1016/j.neuron.2022.06.002.

Overlapping transcriptional programs promote survival and axonal regeneration of injured retinal ganglion cells

Anne Jacobi^{1,2,5}, Nicholas M Tran^{2,3,5}, Wenjun Yan^{2,5}, Inbal Benhar⁴, Feng Tian¹, Rebecca Schaffer², Zhigang He^{1,6}, Joshua Sanes^{2,6,7}

¹F.M. Kirby Neurobiology Center, Boston Children's Hospital, and Department of Neurology, Harvard Medical School, 300 Longwood Avenue, Boston, MA 02115, USA.

²Department of Molecular and Cellular Biology, Center for Brain Science, Harvard University, 52 Oxford Street, Cambridge, MA 02138, USA.

³Department of Molecular and Human Genetics, Baylor College of Medicine, 1 Baylor Plaza, Houston, TX 77030, USA.

⁴Broad Institute of Harvard and MIT, Cambridge, MA 02142, USA

⁵These authors contributed equally to this work

⁷Lead contact

SUMMARY

Injured neurons in the adult mammalian central nervous system often die and seldom regenerate axons. To uncover transcriptional pathways that could ameliorate these disappointing responses we analyzed three interventions that increase survival and regeneration of mouse retinal ganglion cells (RGCs) following optic nerve crush (ONC) injury, albeit not to a clinically useful extent. We assessed gene expression in each of 46 RGC types by single cell transcriptomics following ONC and treatment. We also compared RGCs that regenerated to those that survived but did not regenerate. Each intervention enhanced survival of most RGC types, but type-independent axon regeneration required manipulation of multiple pathways. Distinct computational methods converged on separate sets of genes selectively expressed by RGCs likely to be dying, surviving, or regenerating. Overexpression of genes associated with the regeneration program enhanced both survival and axon regeneration *in vivo*, indicating that mechanistic analysis can be used to identify novel therapeutic strategies.

⁶Corresponding authors (zhigang.he@childrens.harvard.edu; sanesj@mcb.harvard.edu).

AUTHOR CONTRIBUTION

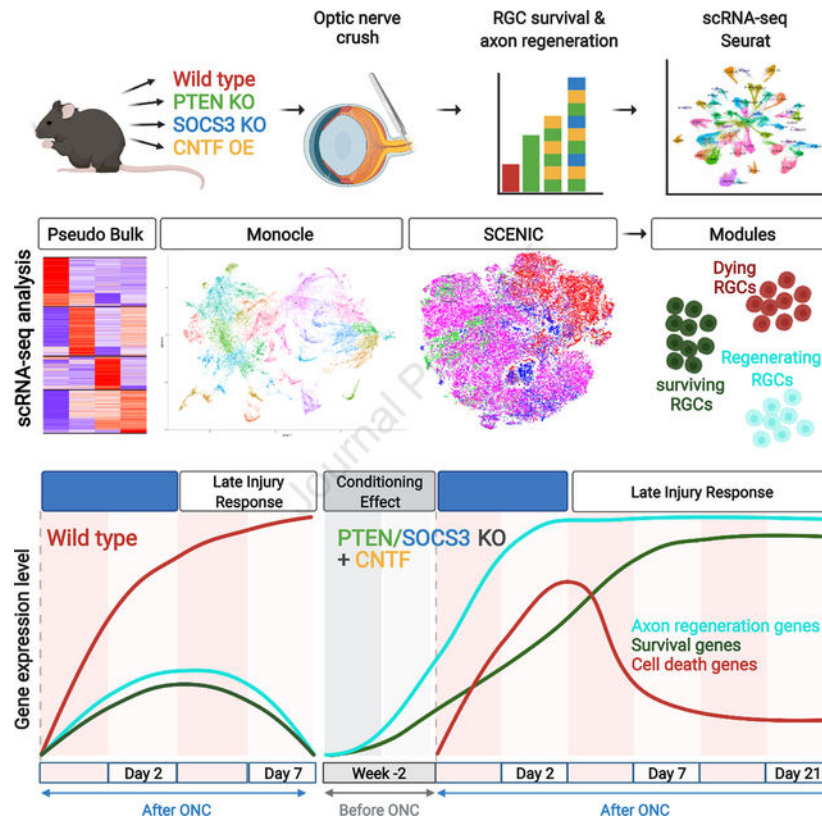
A.J., N.M.T., W.Y., F.T., Z.H and J.R.S. conceived and designed experiments and analyzed data. A.J., N.M.T., I.B., F.T., R.S. performed experiments. Z.H and J.R.S. provided supervision and acquired funding. A.J., N.M.T., W.Y., Z.H. and J.R.S. wrote the paper with input from all authors.

DECLARATION OF INTERESTS

J.R.S. is a consultant for Biogen. Z.H. is an advisor of SpineX, Life Biosciences, and Myro Therapeutics.

Publisher's Disclaimer: This is a PDF file of an unedited manuscript that has been accepted for publication. As a service to our customers we are providing this early version of the manuscript. The manuscript will undergo copyediting, typesetting, and review of the resulting proof before it is published in its final form. Please note that during the production process errors may be discovered which could affect the content, and all legal disclaimers that apply to the journal pertain.

Graphical Abstract



eTOC Blurp

Several interventions promote survival and regeneration of retinal ganglion cells following injury. ScRNA-seq analysis shows that these interventions downregulate a gene expression program associated with cell death and upregulate programs associated with survival and regeneration. Overexpression of some regeneration module genes enhances RGC survival and axon regeneration *in vivo*.

Keywords

axonal regeneration; CNTF; Pten; single cell RNA-seq; Socs3; Wt1

INTRODUCTION

Damage to the axons of central nervous system (CNS) neurons usually leads to permanent functional deficits. Adult CNS neurons have limited capacity to regenerate axons and form new synapses, and in many cases, they die. As Ramón y Cajal wrote a century ago, “In the adult centers, the nerve paths are something fixed, ended, and immutable. Everything may die, nothing may be regenerated. It is for the science of the future to change, if possible, this harsh decree.” (Ramon y Cajal, 1928). In an attempt to meet this challenge, many groups have used models of axonal injury to seek molecules that improve axonal regeneration

and neuronal survival. One intensively studied model is optic nerve crush (ONC), which severs the axons of retinal ganglion cells (RGCs), the projection neurons that transmit visual information from the retina to the rest of the brain. In mice, ~90% of RGCs die during the month following ONC, and few if any of the survivors extend new axons more than a few hundred micrometers past the site of injury (Winter et al., 2021). Using this model, several interventions have been discovered that improve survival and/or axon regeneration, but to date none has been sufficient to restore useful vision.

Our goal in this study was to analyze the molecular effects of these interventions, with the aim of elucidating pathways that promote or constrain neuronal survival and axonal regeneration. To this end, we focused on three manipulations: deletion of genes encoding PTEN (Phosphatase and tensin homolog) and SOCS3 (Suppressor of cytokine signaling 3), and delivery of ciliary neurotrophic factor (CNTF). Each of the three, separately and in combination, have been shown to enhance RGC survival and axon regeneration. The combination of the three is more effective than any one alone, although even in this condition few axons regenerate to their targets (Luo and Park, 2012; Park et al., 2008; Pernet et al., 2013; Smith et al., 2009; Sun et al., 2011; Williams et al., 2020; Xie et al., 2021).

Our strategy relied on high-throughput single cell RNA-sequencing (scRNA-seq). We profiled uninjured, injured, and treated RGCs and classified them into 46 distinct types using recently described criteria (Tran et al., 2019). We showed previously that survival varies nearly 100-fold among types following ONC (Duan et al., 2015; Tran et al., 2019), so we asked whether interventions that enhance survival act selectively on vulnerable or resilient types. Second, we collected RGCs that had regenerated axons and compared them to RGCs that had survived but not regenerated, asking whether interventions promote regeneration of particular types. Next, we used five independent computational methods to analyze gene expression by RGC type, state, time after injury, and intervention, seeking expression patterns that correlated with any of these variables. These methods converged on three groups of genes, one preferentially expressed by RGCs destined to die, another by RGCs that survived but did not regenerate, and a third by RGCs that regenerated axons. These expression modules provide insights into molecular mechanisms that regulate neuronal survival and axon regrowth. Finally, we showed that manipulating several genes from the regeneration module enhances axonal regeneration following ONC, supporting the idea that this strategy can serve as a novel source of therapeutic targets. In a companion paper, we provide further computational and functional analyses of genes that play key roles in the survival of injured RGCs (Tian et al., accompanying paper).

RESULTS

We analyzed effects of three manipulations known to promote survival and axon regeneration from RGCs following ONC: deletion of *Pten*, deletion of *Socs3*, and overexpression of CNTF. PTEN and SOCS3 are endogenous inhibitors of mTOR and Jak/Stat signaling, respectively, and CNTF activates Jak/Stat signaling. As detailed in the Discussion, their modes of action in promoting axon regeneration are incompletely understood. We tested them in three combinations: (1) conditional deletion of *Pten* (P_{CKO}),

(2) conditional deletion of Pten combined with over-expression of CNTF (C/P_{CKO}) and (3) conditional deletion of both Pten and Socs3 combined with over-expression of CNTF (C/PS_{CKO}). Mice also bore the Thy1-YFP line 17 transgene (called YFP17 here; (Feng et al., 2000; Sun et al., 2011), which selectively labels RGCs.

Experiments were initiated by intravitreal injection of AAV2-Cre alone or in combination with AAV2-CNTF in YFP17^{het}Pten^{lox/lox} or YFP17^{het}Pten^{lox/lox};Socs3^{lox/lox} mice. With this route of administration, the AAV2 serotype primarily infects cells of the ganglion cell layer, which contains RGCs and displaced amacrine cells, so deletion is strongly biased to these two cell types. Two weeks following injection, we collected retinas from some of the treated mice and performed ONC on others, then collected retinas 2, 7, or 21 days later (Figure 1A). We also collected retinas from AAV2-Cre-infected YFP17^{het} mice, and uninfected YFP17^{het}Pten^{lox/lox} or YFP17^{het}Pten^{lox/lox};Socs3^{lox/lox} mice (Table S1). In subsequent analyses we found no significant differences in types, type frequencies or gene expression among these latter groups; we therefore pooled data from them and refer to the combined group as “wild-type” (WT) hereafter.

In each case, we collected RGCs by fluorescence-activated cell sorting (FACS) and profiled them by droplet-based scRNA-seq (10X platform; (Zheng et al., 2017)). We identified RGCs based on their expression of pan-RGC markers including the RNA-binding protein, RBPMS, the class 4 POU-domain transcription factors, POU4F1-3 (Brn3a-c), and the glutamate transporter SLC17A6 (VGLUT2). RGCs comprised ~90% of profiled cells. We considered only RGCs hereafter, excluding other cell classes and putative doublets. To estimate the fraction of RGCs that had been infected with AAV2 Cre and/or CNTF, we quantified sequencing reads that mapped to the WPRE element contained in our AAV vectors (see Methods). Such reads were detected in ~80% in all libraries, with no substantial differences among RGC types (Figure S1A). *In situ* hybridization confirmed deletion of Pten from AAV2-Cre-infected P_{CKO} retina (Figure S1B).

Type-independent enhancement of RGC survival

RGC survival was enhanced by all three interventions in the order C/PS_{CKO} > C/P_{CKO} > P_{CKO} > WT, with C/PS_{CKO} preserving >50% of RGCs at 21 days post crush (dpc) (Figure 1B,C). To ask whether these interventions selectively affect specific RGC types or evenly scale across all 46 types, we first clustered RGCs and assigned clusters to atlas types using markers we had identified and validated in wild-type mice (Tran et al., 2019). Most clusters had 1:1 matches with atlas types and >86% of RGCs could be confidently assigned to a type (Figure 1D–F; unassigned cells are discussed further below). Moreover, the specificity of type marker expression was largely retained after crush, though expression was somewhat degraded in WT 7dpc RGCs (Figure S1C). Thus, neither ONC nor interventions had detectable effects on cell type identity.

We then assessed the frequencies of RGC types at each time point and in each condition. Frequencies of RGC types did not differ significantly among groups at 0dpc or 2dpc but some modest differences emerged at 7dpc (Figure 1G). For example, two types of ON-OFF direction selective RGCs (ooDSGCs) and J-RGCs survived disproportionately in some or all groups (Figure S1D, S1E). We also grouped RGCs into subclasses (as defined in(Tran et al.,

2019)) to minimize variability owing to the small numbers of RGCs in some clusters. Again, frequencies were similar across interventions ($r^2=0.70-0.84$), albeit with some exceptions, including disproportionate survival of Cartpt-RGCs (which include ooDSGCs) and T-RGCs (which include J-RGCs) and disproportionate loss of T5-RGCs (Figure S1F–H). Finally, we compared frequency distributions at 7dpc and 21dpc in the C/PS_{CKO} group, to ask whether some types were selectively preserved at later times but saw minimal differences ($r=0.92$; Figure 1H). Taken together, these data show that the improved survival driven by these interventions is observed across most RGC types and that the degree of neuroprotection generally scales with the cell type's innate resilience.

Overcoming type-dependent RGC axon regeneration

We next asked which RGC types regenerated axons following ONC. We first quantified the extent of regeneration by injecting a fluorophore-tagged anterograde tracer intravitreally at 19dpc, fixing and clearing optic nerves at 21dpc, and counting axons in whole mounts. Regeneration was minimal in wild-type mice, but enhanced by all three interventions in the order C/PS_{CKO} > C/P_{CKO} > P_{CKO} (Figure 2A,B) (Duan et al., 2015; Park et al., 2008; Sun et al., 2011). Axonal branching was seldom seen, as previously noted by Luo et al., 2013. This order was the same as that seen for survival (Figure 1B,C), but was not a consequence of enhanced survival in that the increase in regeneration (>100-fold) was far greater than the increase in survival (2–5-fold).

To separate RGCs that regenerated from those that survived but did not regenerate, we used a retrograde labeling method in which we injected a small fluorescently labeled dextran (micro-Ruby, MR) into the nerve stump ~1.5mm distal to the crush site at 20dpc (Zhang et al., 2019). The dextran was taken up by regenerating axons and retrogradely transported to RGC somata, which were also labeled with YFP (Figure 2C,D). Control experiments demonstrated that the method was efficient and specific: most RGCs were labeled in uninjured retina but few if any RGCs were labeled following ONC in wild-type retina (Figure S2A). Thus, this labeling strategy efficiently and specifically marked regenerating axons that, based on dye spread, had extended ~1mm from the crush site (Figure 2D). Conversely, most non-retrogradely labeled RGCs had regenerated minimally if at all. We used FACS to isolate regenerating (MR⁺YFP⁺) and non-regenerating (MR⁻YFP⁺) RGCs 24hrs after tracer injection (Figure S2B), collected single cells in individual wells, and performed scRNA-seq using SmartSeq2 (SS2).

We obtained 120 single RGC transcriptomes from P_{CKO} retinas, 46 from C/P_{CKO} retinas (all MR⁺), and 245 from C/PS_{CKO} retinas (179 MR⁺ and 66 MR⁻). The distribution of RGCs that had regenerated axons differed among the groups: Pten deletion selectively promoted regeneration of alphaRGCs (Figure 2G), consistent with our previous results (Duan et al., 2015), whereas frequencies of regenerating RGCs in the C/PS_{CKO} group approximately mirrored their proportion among survivors (Figure 2 E,F); C/P_{CKO} retinas showed an intermediate value (Figure 2H,I). Combining measurements of the amount of regeneration promoted by P_{CKO} and C/PS_{CKO} (Figure 2B) and the RGC types that regenerate (Figure 2G,I) revealed that similar numbers of regenerating RGCs are alphaRGCs in P_{CKO} and C/PS_{CKO} mice, indicating that most of the “additional” regenerating RGCs in the latter are

non-alphaRGCs. This decline in the fraction of alpha RGCs across interventions – 82% in P_{CKO} , 26% in C/P_{CKO} , and 18% in C/PS_{CKO} – suggests that CNTF and SOCS3 deletion act together to overcome the type-specific barriers seen when only Pten is deleted.

Injury-independent effects of Pten, Socs3 and CNTF

We next undertook a detailed analysis of gene expression changes that result from manipulation of Pten, Socs3 and CNTF, some of which are likely to underlie their beneficial effects. Because we introduced AAV2 vectors two weeks prior to ONC to ensure efficient expression, it was possible that some transcriptional changes preceded injury. This might be akin to the “conditioning effect” observed in dorsal root ganglia, where a “priming” injury to the peripheral branch of the sensory neurons induces growth-promoting transcriptional changes that enhance regeneration of axons following a later injury to the central branch (Neumann and Woolf, 1999; Richardson and Issa, 1984). Therefore, we began by assessing injury-independent effects of these manipulations.

Two weeks after AAV2 injection (i.e., 0dpc), 74 genes were up-regulated in C/P_{CKO} and 51 in C/PS_{CKO} RGCs compared to WT (>1.5-fold, Figure 3A and Table S2). Several of these genes have been annotated as regeneration-associated genes (RAGs) in prior studies (e.g., *Bdnf*, *Stat3*, *Tubb3*; Figure 3A, S3A) (Chandran et al., 2016; Renthal et al., 2020; Yang et al., 2020). For a more comprehensive view, we generated a “RAG score” composed of the 306 differentially expressed (DE) genes selectively expressed by regenerating (retrogradely labeled) RGCs in the C/PS_{CKO} condition (see below, Figure 4). This score was substantially higher in C/P_{CKO} and C/PS_{CKO} RGCs compared to P_{CKO} and WT RGCs (Figure 3B).

A smaller set of genes was downregulated in intact C/PS_{CKO} RGCs relative to controls (16 genes, >1.5-fold, FDR < 0.01). They included *Crhbp*, which inhibits RGC regeneration (Tran et al., 2019) and *Stmn1*, which destabilizes microtubules and therefore could impair axon regeneration (Rubin and Atweh, 2004) (Figure 3C, S3B). Together, these results imply that the interventions we tested may act in part by inducing an axon regeneration program prior to the injury.

Interventions attenuate transcriptional responses of RGCs to injury

To assess gene expression changes following intervention and injury, we first plotted genes that had been identified as being down-regulated (n= 412 - green dots) or up-regulated (n= 359 - magenta dots) in WT mice in our previous study (Tran et al., 2019). Nearly all showed the same responses in the new dataset (Figure 3D), demonstrating (a) that our transcriptomic methods were reproducible and (b) that the 2dpc and 7dpc time points captured both early and late-stage injury response genes from the previous time course (0.5–14dpc).

The global effect of deleting Pten was to attenuate these changes. At 7dpc, 73% of the genes downregulated after ONC in WT mice were expressed at significantly higher levels in P_{CKO} than in WT mice, and 51% of the genes upregulated after ONC in WT mice were expressed at significantly lower levels in P_{CKO} than in WT mice (Figure 3E). No downregulated and only 6% of the upregulated genes displayed the opposite trend. Thus, Pten deletion counteracts injury-induced changes in gene expression. Surprisingly, these injury-induced

changes in gene expression differed little between RGCs from P_{CKO} retina and C/PS_{CKO} retina (Figure 3E–G), suggesting that Pten is the main driver of this mitigation effect.

To determine when Pten acts, we also compared the expression of these DE genes at 0 and 2dpc. Interventions had minimal effect on changes in gene expression at either of these times but counteracted further alterations in expression patterns between 2dpc and 7dpc (Figure 3H). Thus, signaling pathways regulated by Pten deletion divert RGCs from a degenerative path a few days after injury by re-establishing a more “normal” expression program that supports survival.

Genes selectively expressed by regenerating RGCs

Even under conditions that ensure long-term survival, most RGCs fail to regenerate axons (<10% in C/PS_{CKO} retina, calculated from Figures 1C and 2B). To identify genes that might promote regeneration, we compared regenerating (MR⁺) and non-regenerating (MR⁻) RGCs in the C/PS_{CKO} intervention as described above (Figure 2).

Regenerating RGCs selectively expressed 306 genes (>1.5 fold, FDR < 0.01), many of which have been classified as RAG genes (e.g., *Sprr1a*, *Klf6*, *Gap43*; (Bonilla et al., 2002; Jankowski et al., 2009; Latremoliere et al., 2018; Richner et al., 2014; Figure 4A). Gene ontology analysis showed enrichment of pathways related to regulation of cell migration/motility and cell adhesion (Figure 4B, Table S3). In contrast, RGCs that survived but did not regenerate showed enrichment of pathways related to synapse organization and neuronal differentiation, including transcription factors implicated in neurogenesis such as *Neurod2*, *Neurod4* and *Pax6* (Figure 4A, C) (Table S4) (Cherry et al., 2011; Marquardt et al., 2001).

As noted above, C/PS_{CKO} leads to more robust and less type-dependent regeneration of RGCs than P_{CKO} alone. To gain insight into factors that underlie this added benefit, we compared the transcriptomes of regenerating (MR⁺) RGCs in C/PS_{CKO} and P_{CKO} retinas. Unsurprisingly, genes differentially expressed by regenerating P_{CKO} RGCs included marker genes for alphaRGCs (e.g., *Spp1*, *Kcng4*; Duan et al., 2015), consistent with the type-specific regeneration of this group. In contrast, pathways selectively upregulated by the triple intervention were related to immune responses, particularly interferon and cytokine signaling, rather than to specific RGC types, (Figure 4D, E). Thus, while survival appears to be promoted via the re-activation of developmental processes, axon regeneration may require the additional upregulation of RAGs and immune response programs and may contribute to overcoming the type-specific barriers of axon regeneration.

Gene expression programs associated with degenerating, surviving, and regenerating RGCs

In each of the four conditions we analyzed (WT, P_{CKO}, C/P_{CKO}, and C/PS_{CKO}), different proportions of RGCs degenerated, survived and regenerated axons. To identify gene expression programs involved in these three distinct responses, we performed four sets of analyses: (1) We combined all transcriptomes from each intervention at 7dpc and searched for intervention-specific pathways. (2) We used Monocle3 (Qiu et al., 2017) to analyze gene co-expression in RGCs on a single-cell level. (3) We used Seurat (Hao et al., 2021) to assess RGCs that failed to map definitively to a specific type. (4) We used Single-Cell Regulatory

Network Inference and Clustering (SCENIC; Aibar et al., 2017; van de Sande et al., 2020) to identify gene-regulatory networks (GRNs). Remarkably, all four methods converged on a common set of gene modules differentially expressed by degenerating, surviving and regenerating RGCs:

Intervention-dependent gene expression.—To ask whether the three interventions tested regulate distinct genes, we performed pairwise pseudo-bulk differential gene expression at 7dpc and looked for enriched pathways. We combined all RGCs subjected to each intervention and analyzed them in two ways: comparing each condition (WT, P_{CKO}, C/P_{CKO}, and C/PS_{CKO}) at 7dpc to the sum of the others, and each to the next less complex (P_{CKO} to WT, C/P_{CKO} to P_{CKO} and C/PS_{CKO} to C/P_{CKO}). We sorted DE genes for both comparisons into 4 modules by k-means clustering (nclust = 4) (Figure 5A, B, Table S5). In principle, the first comparison would generate intervention-selective genes, while the second would reveal incremental effects of each added manipulation. In fact, however, both comparisons generated similar modules as judged by a hypergeometric test (Figure S4A).

As assessed by gene ontology pathway (GO) analysis, genes in “pseudo-bulk” Module 1 (PB-M1) were associated with pathways related to apoptotic signaling and stress (Figure 5C–E and S5A). Many exhibited a gradual decline across interventions (WT > P_{CKO} > C/P_{CKO} > C/PS_{CKO}; Figure 5C). Conversely, PB-M4 was lowest in WT and increased across treatments (WT < P_{CKO} < C/P_{CKO} < C/PS_{CKO}; Figure 5G, H). Many genes in this module were associated with axonogenesis, axon development, innate immune responses, and hormone signaling (Figure 5F–I). They included *Reelin*, *Cntn2* and RAG genes such as *Nefh* and *Tubb3* (Figures 5I, S5B). PB-M2 and 3 were expressed at highest levels in P_{CKO} and C/P_{CKO} respectively; enriched pathways included those related to synaptic transmission (PB-M2) and cytoplasmic translation (Figure S4B–G).

Together, this comparison shows that deleting Pten from RGCs, augmenting Pten deletion with CNTF and then additionally deleting Socs3 enhances expression of genes associated with survival and regeneration and attenuates expression of genes associated with death and degeneration.

Population-specific gene expression modules.—We next analyzed gene expression at the single-cell level to determine whether transcriptional programs elicited by each intervention were expressed broadly across RGCs or only in specific RGC types. To this end, we reclustered RGCs at 7dpc using Monocle3 (Qiu et al., 2017). The 40 resulting clusters (Figure 6A, Figure S6A) grouped into 6 modules, MO-M1-6. Each included cells from all four conditions (Figure 6B) but occupied distinct (albeit overlapping) regions in UMAP space (Figures 6D–I). MO-M1-3 were closely related to each other (see dendrogram at left of Figure 6A) as were MO-M5 and 6.

MO-M1-3 were enriched in pathways related to synaptic transmission (MO-M1), axonogenesis and axon development (MO-M2, Figures 6J–L, S6D–F). Key genes included *Unc5d*, *Robo2* and *Nrgn*. MO-M3 was expressed by a subset of cells in MO-M1 and 2. These modules showed closest relation to PB-M2 from the pseudo-bulk analysis (Figure 6C). MO-M4 was strongly enriched for genes associated with intrinsic apoptotic and stress

pathways (Figure 6M, S6G, Table S6), and was related to PB-M1 in the pseudo-bulk analysis (Figure 6C). MO-M5 and 6 partially overlapped in UMAP space (Figure 6H, I) and were related to PB-M4 in the pseudo-bulk analysis (Figure 6C). Interestingly, two sets of genes present in PB-M4 were segregated into distinct modules by Monocle: genes associated with hormone and neuropeptide signaling (e.g., *Gal* and *Crh*) and axon regeneration (e.g., *Sprr1a* or *Nefh*) in MO-M5 (Figures S5B, 6N, S6H and Table S6) and genes associated with immune response and cytokine signaling (e.g., *Ifit1* and *Ifit2*) in MO-M6 (Figures 6O, S6I and Table S6). Combined immunohistochemistry and in situ hybridization confirmed that *Gal* (MO-M5) and CART (MO-M2) labeled distinct RGC populations (Figure S6B, C). Thus, all modules were represented in each condition but at different proportions.

Injured RGCs lacking clear type identity.—Although 86% of RGCs could be assigned to specific types or subclasses regardless of intervention or time after injury (Figure 1D), the remainder, comprising 7 clusters (A-G in Figure 1D) could not. To characterize these groups, we compared each of them to all other clusters. DE genes in clusters A-E were closely related to those derived from Monocle analysis: A and E resembled MO-M5 and 6, enriched in genes characteristic of regenerating cells; B resembled MO-M4, characteristic of degenerating cells; and C and D resembled MO-M1, rich in characteristics of synapse organization and transmission (Figure S7A–F). Expression patterns in the other two clusters (F,G), comprising ~17% of this cohort (A-G) were more difficult to interpret. Thus, while the Seurat-based clustering was mostly driven by type identity, the unmapped clusters were largely composed of cells in which “state”- rather than type-driven expression dominated. Importantly, these “states” closely match those observed in the Monocle analysis.

Gene regulatory networks.—To seek transcription regulators of degeneration, survival and regeneration, we used SCENIC (van de Sande et al., 2020) to identify cell-specific gene regulatory networks (GRNs), i.e., groups of transcription factors [TFs] and their predicted target genes, together called regulons (see Methods). We plotted a heatmap of the expression from the top 20 regulons at 7dpc at single cell resolution, revealing sets of cells grouped by regulon activity (Figure 7A), five of which (SC-M1-5) we highlight below.

SC-M1 was enriched for degeneration and cell death-associated TFs including *Atf4*, *Ddit3*, and *Cebpg*, which emerged as key promoters of degeneration in the accompanying study by Tian et al. (accompanying paper). It was related to the death-associated modules derived from pseudo-bulk (PB-M1) and Monocle (MO-M4) analyses, and a majority of its cells were from WT retinas (Figure 7A,B). SC-M2 was enriched for TFs associated with RGC differentiation and neuron development including *Pax6*, *Meis2*, and *Pou4f1* and 2. It was related to the survival-associated modules PB-M2 and MO-M1-3 (Figure 7B). SC-M3 and 4 were related to the regeneration-associated modules PB-M4, MO-M5 and MO-M6. Regeneration associated genes were differentially distributed between these modules: SC-M3 was enriched for canonical RAG TFs (e.g., *Sox11*, *Maz* and *Stat3*), while SC-M4 included TFs associated with innate immunity and interferon signaling (e.g., *Irf1*, 2, and 8) which were regulated in the same RGCs as MO-M6. Target genes regulated by these TFs include additional TFs implicated in immune responses (e.g., *Stat1*), axon growth (e.g., *Creb1*) and axon regeneration (e.g., *Klf6*) (Kole et al., 2020; Ma et al., 2014; Romaniello

et al., 2012; Sun et al., 2015; Wang et al., 2018) emphasizing the complex interactions among TFs in these modules (Table S7). Finally, cells in SC-M5 expressed a combination of genes from SC-M2-4. We speculate that these cells may represent RGCs with modest regenerative ability – for example, RGCs with short regenerating axons (<1 mm), which would not have been labeled by the retrograde labeling technique we used. Consistent with these assignments, target genes in SC-M2 were similar to those selectively expressed in surviving but not regenerating cells in the SS2 dataset (MR⁻) while targets genes in SC-M3 and 4 were like those selectively expressed in the regenerating (MR⁺) group (Figure 7C,D).

While each module contained cells from each intervention, we observed intervention-specific enrichment (Figure S7G), which we quantified by calculating a Regulon Specificity Score (see Methods) for all regulons in each intervention. Consistent with other analyses presented above, the highest scores in WT RGCs were associated with degeneration (with *Ddit3* as the top gene), while C/PS_{CKO} RGCs were enriched for regulons associated with regeneration (with *Wt1* and *Stat3* being the top 2 genes).

We also used SCENIC to measure gene regulatory networks at 0dpc and 2dpc. At 0dpc, the most distinctive group was related to SC-M3 and 4, consisting of RAG and interferon-beta signaling TF's including *Stat1,2,3,5b* and *Irf1,5,7*. It was highly enriched for RGCs from the C/PS_{CKO} condition (Figure S7H), consistent with the finding that these manipulations induce a pro-regenerative “conditioning-like” effect prior to injury (Figure 3). At 2dpc, modules resembling SC-M1 (enriched for cell death related TF's) and SC-M2 (neurodevelopment related TF's) appeared (Figure S7I). Lastly, a group of cells did not clearly associate with a 7dpc module, instead they were enriched for TFs from multiple different states (SC-M6 in Figure S7I), which suggests that these RGCs cells could be in a transitional state.

Taken together, our transcriptional analyses identified expression modules associated with cell states underlying degeneration, survival/initiation of regeneration, and long-distance axon regeneration. Expression modules identified by independent analyses yielded largely consistent groupings. (Degeneration: PB-M2, MO-M4, SC-M1, Seurat B; Survival: PB-M2, Monocle MO-M1/2/3, SC-M2, Seurat C, D, MR⁻; Regeneration: PB-M4, Monocle MO-M5/6, Scenic SC-M3/4, Seurat A, E, MR⁺). Figure 7E provides a schematic that integrates these analyses.

Regeneration-associated genes promote axon regeneration

Manipulation of *Pten*, *Socs3* and *CNTF* enhance RGC survival and regeneration, but have drawbacks as therapeutic targets: *PTEN* and *SOCS3* are tumor suppressors, and recombinant *CNTF* shows minimal effect on its own. A main motivation of our work was the idea that genes downstream of these interventions might provide starting points for new therapeutic developments.

To test this idea, we chose 3 genes selectively expressed by RGCs in a regenerative state. Two, Galanin (*Gal*), and Corticotropin-releasing-hormone (*Crh*), are members of the hormone/neuropeptide signaling group that emerged from pseudo-bulk and Monocle analyses. Galanin positively affects neuronal survival and regeneration upon PNS injury

(Holmes et al., 2000). CRH is a member of the corticotropin-releasing factor family, which includes another known enhancer of RGC survival and regeneration, Urocortin (Tran et al., 2019). The third candidate, *Wt1*, a TF that can act as both tumor suppressor and oncogene (Huff, 2011; Rauscher, 1993; Yang et al., 2007) directs a regulon that is specifically enriched in C/PS_{CKO} RGCs; it has not, to our knowledge, been studied in the context of axon regeneration. All three of these genes are enriched in regenerating (MR⁺) RGCs (Figure 8B). In situ hybridization confirmed expression of *Crh*, *Gal* and *Wt1* (all MO-M5) in regenerating RGCs, while *Cartpt* (MO-M2), a marker of cells that survived but did not regenerate, lacked co-labeling with regenerating RGCs (Figure S8I).

We also tested four additional TFs – *Atf3*, *Atf4*, *Ddit3* and *Cebpg* – based on two criteria: (1) Tian et al. (accompanying paper) showed that they inhibited neuronal survival – that is, deleting them enhanced survival – and (2) *Atf4*, *Ddit3* and *Cebpg* direct regulons specifically enriched in the degeneration module, which was primarily comprised of WT RGCs. Unlike the other three, *Atf3* showed expression in both degenerative and regenerative RGCs (MO-M5 and -M6, Figure S8B), suggesting a dual effect.

We used AAV2 vectors to overexpress (OE) *Gal*, *Crh* and *Wt1*, or to mutate (knock-out, KO) *Atf3*, *Atf4*, *Ddit3* and *Cebpg* by introduction of gRNAs in Cas9-expressing RGCs. We injected AAV2 intravitreally 2 weeks prior to ONC and quantified RGC axon regeneration via anterograde tracing injected 2 days prior to collection (Figure 8A). Efficiency of OE or KO was demonstrated previously (Tran et al., 2019) and repeated here for selected genes using FISH (Figure S8A). The three overexpression interventions each showed a positive effect on the number of regenerating axons out to 1.5mm from the crush site (Figure 8C, D) and also enhanced RGC survival (Figure 8E, F). Interestingly, among predicted targets of *Wt1*, nearly 20% (9/52) were membrane-associated genes implicated in axon outgrowth, such as *Ch11*, *Cntn2* (Katic et al., 2014; Suter et al., 2020) (Table S7), underlining its potential role as a regulator for axon regeneration. In contrast, although *Atf3*, *Atf4*, *Ddit3* and *Cebpg* all enhance survival following ONC (Tian et al.; accompanying paper), they had no effect on regeneration driven by *Pten* deletion (Figure S8C, D), emphasizing the distinct control of these two processes.

Finally, we manipulated six targets in combination with P_{CKO} to determine whether their pro-regenerative effects are synergistic to *Pten* deletion. However, neither overexpression of *Gal*, *Wt1* or *Crh* nor deletion of *Atf4*, *Ddit3* or *Cebpg* led to regeneration beyond the level observed with *Pten* deletion alone (Figure S8E–H and 8G,H). In contrast, *Atf3* knockout dramatically attenuated P_{CKO} induced axon regeneration (Figure 8H).

DISCUSSION

Following ONC in mouse, most RGCs die and hardly any of the survivors extend their axons beyond the injury site. This model has been used to seek interventions that can enhance survival and promote regeneration, but none to date has been shown to restore useful vision (He and Jin, 2016; Williams et al., 2020). The goal of this study was to investigate ways in which three of these interventions, described below, act and to identify the core molecular programs associated with axon regeneration, with the aim of finding novel

therapeutic approaches. To this end we pretreated retinas in three ways prior to ONC, then used high throughput scRNA-seq to assess their effects. Our results fall into three groups. First, we analyzed the cell type-specificity of these interventions. All RGCs are similar in many respects but can be divided into ~46 types based on morphological, physiological and molecular differences. We and others have shown that the extent of survival without intervention varies dramatically among these 46 RGC types (Bray et al., 2019; Duan et al., 2015; Tran et al., 2019). Here, we asked whether the interventions selectively affect some of them or whether their benefits are equally distributed across types. Second, we analyzed gene expression programs activated or repressed by the interventions. Finally, we tested genes identified through expression analysis by overexpression or deletion *in vivo* and found that some indeed promoted regeneration.

Role of Pten, Socs3 and CNTF in neuroprotection and axon regeneration

The interventions we used were conditional deletion of the cytoplasmic phosphatase Pten, conditional deletion of the negative regulator cytokine signaling Socs3, and overexpression of the cytokine and neurotrophic factor CNTF. All interventions used AAV2 vectors injected intravitreally to manipulate target gene expression in a relatively RGC-selective manner.

PTEN antagonizes PI3-kinase by dephosphorylating lipid substrates of PI3-kinase. A major consequence of Pten deletion is the activation of a protein kinase, AKT, which in turn activates mTOR (Jaworski and Sheng, 2006; Nieuwenhuis and Eva, 2022). Earlier studies showing that Pten deletion enhanced RGC survival and regeneration provided evidence that mTOR activation is required for the effect (Park et al., 2008; Sun et al., 2011), but they did not address whether it is sufficient. PTEN and AKT also modulate other pathways (Hill and Wu, 2009; Manning and Cantley, 2007; Morgan-Warren et al., 2013) and may act in the nucleus as well as cytoplasmically (Planchon et al., 2008). The role of PTEN in axon regeneration likely involves some of these additional pathways, as interventions that more selectively activate mTOR are less effective in eliciting regeneration than Pten deletion (Duan et al., 2015; Park et al., 2008).

The second intervention was to deliver ciliary neurotrophic factor (CNTF) in parallel with Pten deletion. Addition of CNTF significantly increased RGC axon regeneration (Figure 2A, B). CNTF is a cytokine that acts in part through JAK/STAT signaling (Peterson et al., 2000) and has been shown to be a potent neurotrophic factor in multiple contexts (Fudalej et al., 2021; Richardson, 1994). On its own, CNTF gene therapy primarily acts cell-non-autonomously in retinal glial and immune cells (Müller et al., 2007; Xie et al., 2021). In combination with SOCS3 deletion, however, it most likely has both direct and indirect effects on RGC survival and axon regeneration (Smith et al., 2009; Xie et al., 2021). We induced CNTF-expression selectively in neurons of the ganglion cell layer (RGCs and amacrine cells) using the AAV2/2 serotype, and the CNTF receptor (*Cntfr*) is expressed by RGCs, but we cannot exclude the possibility that the effects we saw involve additional cell types.

The third intervention was deletion of Socs3, in combination with Pten deletion and CNTF overexpression. The combined treatment further enhanced RGC axon regeneration and survival, consistent with previous studies (Sun et al., 2011). SOCS3 acts in part as an

inhibitor of the JAK/STAT signaling pathway by blocking JAK2 activity (Babon et al., 2012; Kershaw et al., 2013), which in turn can decrease the responsiveness of neurons to injury-induced cytokine signaling including the activity of CNTF (Croker et al., 2008). Additionally, SOCS3 has been shown to negatively regulate interferon (IfN) and other cytokines (Yu et al., 2018). Sun et al., (2011) provided evidence that this pathway is required for the regeneration-promoting effect of SOCS3 in that its effect is lost when Stat3 is also mutated. However, as with Pten, other pathways likely contribute to Socs3-dependent axon regeneration.

Overcoming type-selective survival and regeneration

RGC types vary dramatically in resilience, with the most resilient and vulnerable types showing ~99% and ~1% survival at 14dpc, respectively (Duan et al., 2015; Tran et al., 2019). These molecular differences allowed us to identify targets for neuroprotection (Tran et al., 2019). Here we asked whether neuroprotective and pro-regenerative interventions also selectively affected specific types, which could confer a similar opportunity for target discovery.

In fact, the interventions enhanced survival of most RGC types to similar extents. A few types were rescued with modest selectivity; they included J-RGCs and two types of ooDSGCs. All of these types are inherently vulnerable to ONC (Tran et al., 2019). Conversely, RGCs of the T5 subclass were somewhat poorly rescued. Nonetheless, our overall conclusion is that these interventions showed little selectivity; most RGC types benefited to a similar extent.

In contrast, the effects on regeneration varied among interventions. Pten deletion led to selective regeneration of alphaRGCs, consistent with our previous results (Duan et al., 2015), while also overexpressing CNTF decreased the selectivity and the additional deletion of Socs3 almost completely overcame these type-specific barriers. These results suggest that broad and extended long-distance regeneration of CNS neurons might only be possible when manipulating multiple genes/factors simultaneously.

Distinct programs drive death, survival and regeneration

ScRNA-seq revealed transcriptional programs associated with distinct cell states across conditions. In each analysis, three main gene expression modules were evident: one selectively expressed by RGCs that were degenerating or vulnerable, a second by RGCs that survived but failed to extend axons >1mm, and a third by RGCs that not only survived but also extended axons at least 1 mm past the crush site. Figure 7E schematizes the changes in these programs over time, in wild-type mice and following interventions. In wild-types, genes in all three modules are upregulated after ONC, but whereas the death module continues to increase, initial increases in the survival and regeneration modules are not maintained (left panel). In striking contrast, increases in the death module are transient in C/PSCKO retina, but increases in survival and regeneration modules are dramatic and sustained (right panel). Patterns in PCKO (middle panel) and C/PCKO, (not shown) are intermediate. Together, these patterns give a qualitative sense of how the interventions promote neuronal survival and axon regeneration.

Having mapped these modules, we identified gene expression programs associated with each group.

Vulnerable and dying RGCs.—RGCs in this group expressed genes commonly associated with intrinsic apoptotic signaling and stress response pathways. They included *Ddit3* (CHOP) and *Cepbg*, which are key negative regulators of RGC survival (Tian et al., accompanying paper; Hu et al., 2012; Syc-Mazurek et al., 2017). Most of these genes are globally upregulated by RGCs, including those that are relatively resilient (see also Tran et al., 2019).

Surviving RGCs.—RGCs in this group suppress the degenerative program and upregulate genes implicated in neuronal development, axonogenesis, synaptic organization and synaptic function. Reactivation of developmental genes has been noted in regenerative CNS neurons (Hilton and Bradke, 2017; Poplawski et al., 2020) and synaptic/neuronal activity promotes axon regeneration and functional connectivity following injury as well as suppression of apoptotic signaling pathways (Enes et al., 2010; Hilton et al., 2022; Léveillé et al., 2010; Li et al., 2016; Lim et al., 2016; Tedeschi et al., 2016; Williams et al., 2015; Zhang et al., 2019). We speculate that some of those cells may be in a resting state, initiating a regenerative program that failed or in an early regenerative state which at the point of collection only enabled short distance regeneration.

Regenerating RGCs.—These RGCs suppressed injury response and activated axonogenesis-related genes, but additionally activated other pathways, which included previously RAGs (Abe and Cavalli, 2008; Chandran et al., 2016); genes related to the immune response, which have been shown to induce RGC axon regeneration (Benowitz and Popovich, 2011; Bollaerts et al., 2017; Schwartz and Raposo, 2014; Sun et al., 2011), and genes involved in hormone and neuropeptide function. Previous studies have implicated an essential role of hormones in axon growth (Baudet et al., 2009) and neuronal survival (Sanders et al., 2005) during development, and several are known to be upregulated following axotomy of and/to enhance axon outgrowth from peripheral neurons (Holmes et al., 2000; Palkovits, 1995; Tran et al., 2019; Yuan et al., 2010). The appearance of a coordinated neuropeptide-related response in injured CNS neurons, which generally fail to regenerate, along with the gene therapy results (Figure 8, discussed below) is noteworthy from a translational perspective, in that peptides have been used as safe and effective therapeutics in multiple indications.

Stepwise establishment of responses to injury

By collecting and analyzing cells at several time points, we followed the emergence of gene expression programs regulated by *Pten*, *Socs3* and *CNTF*. Identifying the dynamics of these programs helps narrow the window of opportunity for therapeutic strategies.

Prior to injury.—We initiated downregulation of *Pten* and *Socs3* and overexpression of *CNTF* two weeks before ONC. Although our aim was to ensure that gene expression changes had occurred by the time of injury, this protocol provided an opportunity to distinguish injury-dependent from injury-independent effects. Prior to injury the triple

intervention (C/PS_{CKO}) led to upregulation of pro-regeneration “RAG” genes previously identified in both peripheral and central nervous systems (Renthal et al., 2020; Yang et al., 2020). These changes mimic the “pre-conditioning” effect seen in DRG injury models (Cai et al., 1999; Hannila and Filbin, 2008; Neumann and Woolf, 1999; Richardson and Issa, 1984). Down-regulated genes, which were fewer in number, included known inhibitors of axon regeneration (*Crhbp*) and microtubuli stabilization (*Stmn1*) (Rubin and Atweh, 2004; Tran et al., 2019). Our data suggests that these changes act in part prior to injury, a measure of little therapeutic value. Despite that caveat, *Pten* and *Socs3* deletion or CNTF overexpression post-injury do elicit potent axon regeneration in some injury models (Danilov and Steward, 2015; Du et al., 2015; Hellström et al., 2011; Sun et al., 2011).

Shortly after the injury.—At 2dpc, the interventions showed little effect on the injury responses of RGCs (Figure 3H), although SCENIC analysis identified a modest enhancement of regeneration-associated expression patterns compared to those at 0dpc. Thus, even though *Pten*, *Socs3* and CNTF levels have been affected prior to injury, activation of the degeneration program observed in the absence of interventions is not substantially attenuated by the interventions nor are survival programs activated early after injury.

One week after the injury.—Between 2dpc and 7dpc, all interventions exerted dramatic effects. *Pten* deletion mitigated the general injury response, by attempting to re-establish the gene expression milieu of uninjured RGCs. RGCs additionally became more distinct in their gene expression profile, with survival and regenerative programs robustly activated. This separation was still apparent at 21dpc, showing that the regenerative state achieved in the first week after the injury is maintained over time.

In short, we demonstrate multiple temporal phases in the effects of intervention. First, there is a modest upregulation of a regenerative state prior to and independent of injury. Second, little change occurs during the first two days after ONC. Third, further degenerative changes are prevented, and survival and regeneration programs are activated between 2 and 7dpc. Finally, expression changes are modest between 7 and 21dpc.

Promoting axon regeneration

To test if genes correlating with regeneration contribute to this process, we used gain-of-function experiments in which we overexpressed genes present in the regeneration modules. Overexpression of three such genes – *Crh*, *Gal* and *Wtl* – resulted in significant axon regeneration. In experiments reported here, we infected RGCs with AAVs prior to injury to ensure robust expression by the time of ONC; further studies will be required to determine whether these manipulations are effective if administered after injury.

Neuropeptides.—A key pathway in the “regeneration modules” was annotated as involving hormone and neuropeptide secretion and signaling. We chose two candidates from this group to test - *Crh* and *Gal*. Both promoted axon regeneration, as did another peptide, urocortin (*Ucn*), that we previously identified as selectively expressed by resilient cells (Tran et al., 2019). Further studies will be needed to identify the cellular pathways

they affect and to determine whether signaling is cell-autonomous or non-autonomous. Signaling could be direct to RGCs as the Crh receptor (*Crhr1*) is expressed in a subset of them. In contrast, we did not detect the expression of the receptors for Galanin (*GalR1*, *GalR2* and *GalR3*) in RGCs, suggesting GAL may act cell-non-autonomously or through yet unidentified receptors. Other neuropeptides (e.g., PACAP; Baskozos et al., 2020) and monoamines (e.g., serotonin; Kingston et al., 2021) have also been shown to alter axon regeneration capability.

Wt1.—Wt1 has been shown to exert anti-apoptotic functions in several cell types (Huff, 2011; Loeb, 2006; Yang et al., 2007) including developing RGCs (Wagner et al., 2002). Moreover, Wt1 regulates expression of POU4F2 (Brn-3b), a key regulator of RGC maturation (Wagner et al., 2002) and binds to promoters of multiple genes implicated in axonal regeneration (Gao et al., 2019; Hartl and Schneider, 2019). More recently, studies revealed that Basp1, a growth cone associated protein, is a binding partner of Wt1 (Hartl and Schneider, 2019). In our SCENIC analysis, we noted that genes potentially regulated by and co-expressed with Wt1 include a high proportion of membrane-associated genes implicated in axon outgrowth. Like Pten and Socs3, Wt1 itself is an oncogene and tumor suppressor gene, and therefore problematic as a therapeutic candidate. Notwithstanding, the genes it regulates may provide insights into the control of neuronal survival and axon regeneration as well as a source of novel candidates.

Atf3, Atf4, Ddit3 and Cebpg.—This set of 4 TFs play key roles in coupling effects of axonal injury to neuronal death; in their absence, neurodegeneration is attenuated (Tian et al., accompanying paper). We observed no effect of deleting any of them on axonal regeneration, supporting the hypothesis that programs regulating survival and regeneration are distinct. Likewise, deletion of *Atf4*, *Ddit3* or *Cebpg* did not significantly affect the ability of Pten deletion to promote axonal regeneration. On the other hand, Pten deletion was no longer able to promote regeneration when *Atf3* was also deleted. This result supports the idea that Atf3 promotes axonal regeneration of injured peripheral sensory neurons (Renthal et al., 2020) but is seemingly inconsistent with its role in promoting RGC death (Tian et al., accompanying paper). However, its appearance in both degenerative and regenerative modules (MO-M5 and -M6) suggests that unlike the other TFs we assessed it plays a dual role at successive stages of the injury response.

STAR★METHODS

LEAD CONTACT

Further information and requests for resources and reagents should be directed to and will be fulfilled by the Lead Contact, J.R.S. (saneshj@mcb.harvard.edu).

RESOURCE AVAILABILITY

Requests for resources and reagents should be directed to and will be fulfilled by the Lead Contact, J.R.S. (saneshj@mcb.harvard.edu).

DATA AND SOFTWARE AVAILABILITY

Submission of all the raw and processed datasets reported in this study has been initiated to the Gene Expression Omnibus (GEO). The accession number for the sequencing data reported in this paper is GEO: GSE202155. The single cell data can be visualized in the Broad Institute's Single Cell Portal at https://singlecell.broadinstitute.org/single_cell/study/SCP1846.

EXPERIMENTAL MODEL AND SUBJECT DETAILS

Animals—All animal experiments were approved by the Institutional Animal Care and Use Committees (IACUC) at Harvard University and Children's Hospital, Boston. Male and female mice were used interchangeably. Mice were maintained in pathogen-free facilities under standard housing conditions with continuous access to food and water. All experiments were carried out in adult mice from 4 to 12 weeks of age. The following mouse strains were used:

Pten loxP/loxP (JAX # 006440)

Pten loxP/loxP Socs3 loxP/loxP (Sun et al., 2011)

Thy1-stop-YFP Line #17 (Sun et al., 2011).

Vglut2-Cre (JAX #0288663)

Rosa26-LSL-Cas9 knockin (JAX #024857).

C57Bl/6J (JAX #000664)

METHOD DETAILS

Optic Nerve Crush—Mice were anesthetized with ketamine/xylazine (ketamine 100–120 mg/kg and xylazine 10 mg/kg). We performed optic nerve injury as previously described (Park et al., 2008; Tran et al., 2019). Briefly, the optic nerve was exposed intraorbitally and crushed with fine forceps (Dumont #5 FST) for ~2s approximately 0.5–1mm behind the optic disc. Eye ointment was applied post-operatively to protect the cornea.

Intravitreal injection of AAV—Mice were anaesthetized with ketamine/xylazine (ketamine 100–120mg/kg and xylazine 10 mg/kg) and injected intravitreally with ~2µl of volume of AAV2 (in 1x PBS) carrying the gene of interest driven by a CAG promoter, or an sgRNA driven by a U6 promoter. Concentration of viruses was adjusted to $\sim 5 \times 10^{12}$. For injections, we first removed ~2µl intravitreal fluid from the eye with a sterile glass micropipette. Another glass micropipette or a 33-gauge Hamilton syringe was then inserted through the sclera about 0.5 mm posterior to the limbus and into the vitreous chamber without touching the lens. AAV solution (~2µl) was injected. After injection, antibiotic ophthalmic ointment was applied, and mice were warmed on a heating pad until fully awake.

Anterograde tracing of regenerating axons—To assess axon regeneration, axons were anterogradely labeled by intravitreal injection of CTB conjugated with Alexa-647 (Life

Technology) 48 hours before sacrifice. After 4% PFA perfusion, heads were post-fixed overnight in 4% PFA. Optic nerves were micro-dissected and meninges surrounding the nerve were removed. Nerves were then cleared using reagents and protocol provided from Visikol®. Briefly, nerves were dehydrated with 100% methanol for 4 minutes and then transferred into Visikol Histo-1 solution for overnight incubation at 4°C. The next day the nerves were incubated in Visikol Histo-2 solution for at least 2 hours before mounting them in Visikol Histo-2 solution and imaged with the LSM710 confocal microscope. We observed little axonal branching or turning distal to the crush site, consistent with a previous report that used 3D reconstructions (Luo et al., 2013). Thus, although we cannot exclude the possibility of branching in heavily labeled areas proximal to the crush site, we conclude that the number of axons is roughly equivalent to the number of RGCs that regenerated axons.

In some cases, we used an iDISCO tissue clearing method (Renier et al., 2014). In this method, optic nerves were incubated in the dark for 0.5h with 80% tetrahydrofuran (THF, Sigma-Aldrich 360589-500ML)/H₂O and then transferred to 100% THF for 1h. Nerves were then incubated in Dichloromethane (DCM, Sigma-Aldrich 270997-1L) for 20min and switched to dibenzyl ether (DBE, Sigma-Aldrich 33630-250ML) until they were completely transparent (at least 3h).

Optic nerves showing incomplete crush as evidenced by continuous labeling of axons through the chiasm and/or a different morphology than regenerating axons (pearls on a string) were excluded from the analysis; they comprised a low percentage of all nerves analyzed (Tran et al., 2019).

Retrograde labeling of regenerating RGCs—Retrograde labeling of regenerated RGCs was performed as described previously (Zhang et al., 2019), using micro-Ruby or TexasRed (ThermoFisher #D7162 or #D3328), both of which are 3kDa dextrans conjugated to biotin. Twenty days after ONC, mice were anesthetized and placed in a stereotaxic frame. The crushed optic nerve was exposed using a superior temporal intraorbital approach by drilling a hole into the skull and removing overlying brain tissue. After exposing the optic nerve ~1.5 mm distal to the crush site, we cut the nerve with a fine blade and delivered 100–300 nL of a 5% micro-Ruby or TexasRed solution diluted in sterile PBS to the stump. We then placed a small piece of gelfoam (Fisher Scientific) soaked in this 5% dextran solution on the cut nerve stump. The scalp was sutured, and animals recovered on a heating pad until they regained consciousness. For single cell isolation and SS2, mice were injected with micro-Ruby and perfused ~24 hours after delivery.

Cell preparation and FACS—We used the methods detailed in Tran et al. (2019) for dissociation and FACS sorting of RGCs. Briefly, retinas were dissected in AMES solution (equilibrated with 95% O₂/5% CO₂), digested in papain, and dissociated to single cell suspensions using manual trituration in ovomucoid solution. For a concentration of 10 million cells per 100µl, 0.5µl of 2µg/µl anti-CD90 (conjugated to various fluorophores) (Thermo Fisher Scientific) was used to stain (15 minutes incubation), washed with an excess of media, spun down and resuspended again in AMES+4%BSA to a concentration of ~7 million cells per 1 ml. Just prior to FACS the live cell marker calcein blue was added. RGCs were collected based on high CD90, GFP and, in some cases, micro-Ruby co-expression.

For 10X experiments, cells were collected into ~100ul of AMES+4%BSA per 25,000 sorted cells. Following collection cells were spun down and resuspended in PBS+0.1% non-acetylated BSA at a concentration range of 500–2000 cells/ul for droplet-based scRNAseq per manufacturer's instructions (10x Chromium). For SS2 experiments, single cells were collected into 96 well plates filled with 5µl of TCL lysis buffer, containing 1% BME, spun down and frozen at –80°C till further processing.

RNA-sequencing

3 'droplet-based scRNA-seq: Single cell libraries were prepared using the Single-cell gene expression v2/v3 kit on the Chromium platform (10X Genomics, Pleasanton, CA) following the manufacturer's protocol. Briefly, single cells were partitioned into Gel beads in EMulsion (GEMs) in the Chromium instrument followed by cell lysis and barcoded reverse transcription of RNA, amplification, enzymatic fragmentation, 5' adaptor attachment and sample indexing. On average, approximately 8,000–12,000 single cells were loaded on each channel and approximately 3,000–7,000 cells were recovered. Libraries were sequenced on Illumina HiSeq 2500, or NovaSeq platforms (Paired end reads: Read 1, 26 bases, Read 2, 98 bases).

Retrograde labeled RGCs: Smart-seq2: We generated RNA-Seq libraries using a modified Smart-seq2 method (Picelli et al., 2014) with the following minor changes: Before running RT, RNA was purified using 2.2X SPRI-beads (Beckman Coulter, A3987) followed by 3 wash steps with 80% EtOH, elution in 4µl of RT primer mix and denatured at 72°C for 3 min. Six microliters of the first-strand reaction mix, containing 0.1µl SuperScript II reverse transcriptase (200 U/µl, Invitrogen), 0.25µl RNase inhibitor (40 U/µl, Clontech), 2µl Superscript II First-Strand Buffer (5x, Invitrogen), 0.1µl MgCl₂ (100 mM, Sigma), 0.1µl TSO (100 µM) and 3.45µl Trehalose (1M), were added to each sample. Reverse transcription reaction was carried out by incubating at 50°C for 90 min and inactivation by incubation at 85°C for 5 min. After PCR preamplification, PCR was purified using 0.8X of AMPure XP beads (Beckman Coulter), with the final elution in 12µl of EB solution (Qiagen). For tagmentation the Nextera DNA Sample Preparation kit (FC-131-1096, Illumina) was used, and final PCR was performed as follows: 72°C 3 min, 95 °C 30 s, then 12 cycles of (95°C 10 s, 55°C 30s, 72°C 1min), 72°C 5min. Purification was done with a 0.9X of AMPure XP beads. Libraries were diluted to a final concentration of 2nM, pooled and sequenced on Next-Seq 500 or Nova-Seq, 50bp paired end.

Whole mounts: Eyes were either collected from animals intracardially perfused with 15–50ml of 4% paraformaldehyde (PFA), and post-fixed for an additional 15 minutes, or dissected from nonperfused animals and immersion fixed in 4% PFA for 30 minutes. Eyes were transferred to PBS until retinas were dissected.

To immunostain whole mounts, retinas were incubated in blocking solution (5% normal serum, 0.3% Triton-X100 in PBS) for 3 hours, followed by incubation with primary antibodies (in blocking solution) for 5–7 days, and secondary antibodies (in PBS) overnight. All incubations were done at 4°C with gentle rocking.

Jam2 expression was assessed by fluorescent *in situ* hybridization using a hybridization chain reaction method (<https://www.moleculartechnologies.org/>). Probes of 15–20nt length were generated by Molecular Instruments. Retinas were dissected in RNase-free 1xPBS and immediately washed 2 × 5min in PBST (1xPBS + 0.1% Tween20) on ice. Retinas were then dehydrated using MeOH – PBST mix series (0%, 25%, 50%, 75% and 100% of MeOH), each step for 15min on ice. Retinas were incubated in 100% methanol overnight at –20°C. After rehydration on ice the next day (inverted order of previous dehydration) and 10min incubation in PBST at RT, retinas were incubated for 30min at 37°C for pre-hybridization. Then retinas were incubated in hybridization buffer including the probe (2.5nM) overnight at 37°C. After hybridization retinas were washed 4 × 15min with wash buffer (at 37°C) followed by 2 × 5min in 5x saline-sodium citrate (SSC) at room temperature (RT). The amplification step was performed with amplifiers B1 or B2 for 24hrs at RT in the dark. Finally, retinas were immunostained for RBPMS as above and mounted.

Retinal sections: Eyes were collected and retinas dissected as described above. Retinas were then sunk in 30% sucrose, embedded in tissue freezing media, and cryosectioned at 20µm. For IHC, slides were incubated for 1 hour in protein block, primary antibody incubation overnight, and secondary antibodies for 2–3 hours. Initial block and secondary antibody incubation were done at RT and primary antibody incubation at 4°C.

For FISH, probes were either obtained from Molecular Instruments (*Atf4*, *Ddit3* and *Jam2*) and used as described previously (Li et al., 2020). All other probes were generated, and FISH was performed as described in Tran et al. (2019).

Design of overexpression and knockdown vectors: Vectors were cloned by Synbio Technologies (Monmouth Junction, NJ 08852) using the pAAV-hSyn-hChr2(H134R)-EYFP plasmid (Addgene #26973) to replace the hChr2(H134R)-EYFP with the gene target sequence for over expression experiments. Virus of serotype AAV2/2 was then generated by the Boston Children’s Hospital Viral Core. For Crispr mediated KD a modified AAV-U6-sgRNA-hSyn-mCherry plasmid (Addgene #87916) was used. The AAV2-based Crispr/Cas9 approach we employ here has been established as an effective modality for somatic knockdown in adult mouse RGCs (Hung et al., 2016). To account for possible off target effects, we delivered a mix of 5 AAV2 single-guide RNA (sgRNA) expression vectors to the eyes of mice that express Cas9 specifically in RGCs (VGlut2-Cre; LSLCas9-eGFP), which lead to high infection rates as described previously and indicated in Figure S8A. Vectors and sequences used for manipulation experiments are displayed in Table S8.

Computational Methods

Reads alignment of 3 ‘droplet-based scRNA-seq data: Sequenced reads were demultiplexed using cellranger (version 2.1.0, 10x Genomics) “mkfastq” function and aligned to mouse genome mm38 with modified transcriptome (Tran et al., 2019) using cellranger “count” function.

Clustering and cell type identification in 3 ‘droplet-based scRNA-seq data: The generated gene count matrix was processed using the R package “Seurat” (Version 4.0.1).

Both the standardized log normalization and the “sctransform” method were used for processing. Briefly, the gene expression matrix generated by log normalization and scaling with a factor of 10000 were used for differential gene expression analysis and data visualization, while the sources of variation for each intervention at each time point were removed using the “sctransform” framework and clustering was performed based on the corrected values. The 2000 top ranked common features among interventions at each time point were selected using function “SelectIntegrationFeatures”. The canonical correlation analysis-based data Integration method (function “IntegrateData”) was applied using each and all the interventions without optic nerve crush as the reference dataset. Principal Component analysis (PCA) was performed, and the top 100 PCs were used to construct a shared nearest neighbor (SNN) graph, with k=100 as the k-nearest neighbors. The Louvain algorithm with multilevel refinement algorithm was used for modularity optimization in identifying the clusters. In the first round of clustering, canonical retinal cell class markers were used to identify major cell classes in the dataset including amacrine cells and RGCs. Only RGCs were retained for further analysis, using the pipeline described above. Results were evaluated based on number of distinct marker genes in each cluster as well as their correspondence to the RGC type prediction using machine learning algorithm XGBoost (See below for details). A resolution of 3 was chosen as the clustering parameter in the function “FindClusters” based on the integrated SNN.

To identify RGC types in each cluster, two methods were used. First, a machine learning algorithm “XGBoost” was applied as described previously (Yan et al., 2020; van Zyl et al., 2020) to build the RGC type predictor based on the RGC atlas dataset (Tran et al., 2019). Confusion matrices were generated between the predicted result and clusterings at various resolutions. High consensus was observed among results, with subtle differences in a small set of clusters. In those cases, differential gene expression (DGE) analysis was performed to verify the sub-division of certain types using the “MAST” method by “Seurat” function “FindMarkers” based on the log normalized data. Clusters were kept as separate if more than 5 differentially expressed (DE) genes were identified in both groups with over 10% expression in either cluster and over 0.5 log-fold change. Otherwise, the clusters under evaluation were merged or a lower resolution was chosen. As a second measure to ensure the accuracy of RGC type identification, expression of type marker genes from (Tran et al., 2019) was inspected in each cluster. When measuring at the level of subclasses, the composition of RGC types was defined as in Figure 2J in Tran et al., 2019.

Detecting of Cre/CNTF transcript expression in dataset: A separated alignment of the reads was performed using the same cellranger count function but using a reference genome to which the WPRE (Cre-HAtag-WPRE) sequence, shared by both AAV vectors (Cre and Cntf) had been added.

Cre-HAtag-WPRE sequence:

```
tccaattactgaccgtacacaaaatttgctgcattaccggctgatgcaacgagtgatgaggttcgcaagaacctgatggacatgtt
cagggatcgccaggcgtttctgagcaccctggaaaatgctctgtccgttgccggctgtggcgccatggtgcaagttgaataac
cggaaatggtttcccgcagaacctgaagatgttcgctgattatcttctatctcagggcgcgggtctggcagtaaaaactatccagca
acattggccagctaaacatgcttcacgtcgtccgggctgccacgaccaagtacagcaatgctgtttcactggttatcgccggc
atccgaaaagaaaacgttgatgccggtgaacgtgcaaaacaggctctagcgttcgaacgactgatttcaccaggttcgttactca
```

tgaaaaatagcgatcgctgccaggatatacgaatctggcattctggggattgcttataaacacctgttacgtatagccgaaattgcca
 ggatcagggttaaagatatctcacgtactgacgggtgggagaatgtaatccatattggcagaacgaaacgctggttagcaccgcag
 gtgtagagaaggcacttagcctgggggtaactaaactggtcgagcggatgattccgtctctggtgtagctgatgatccgaataactac
 ctgtttgccgggtcagaaaaatggtgtgcccgcacctctgccaccagccagctatcaactcgcgcctggaagggattttggaag
 caactcatcgattgatttacggcgtaaggatgactctggtcagagatactggcctggcttgacacagtgccctgctggagccgc
 gcgagatatggcccgcgctggagttcaataccggagatcatgcaagctggtggctggaccaatgtaaattgcatgaactatacc
 gtaacctggatgaaacagggcaatggtgctgctggaagtgccgattaccatacagattccagattacgcttaaTCT
 AGAGTTCGACCTGCAGAAGCTTatcgaTaatcaacctctgattacaaaattgtgaaagattgactggtattcttaac
 tatgttctcttttacgctatgtggatacctgctttaatgcctttgatcatgctattgcttccgtatggcttctctctctctgataa
 atcctggtgctgctctttatgaggagttggtgcccgttcaggcaacgtggcgtggtgctgactgtgttctgacgcaacccccac
 tgggtggggcattgccaccacgtcagctccttccgggacttccgttccccctccctattgccacggcggaaactcatgccgcctg
 ccttggccgctgctggacaggggctcggctgtgggactgacaattccgtggtgtgctggggaagctgacgtcctttccatgctg
 ctgcctgtgtgccactgagttctgcgaggactcctctgctacgtccctcggccctcaatccagcggaccttctcccgcg
 cctgctgccgctctcggcctctcccgctcttcgcttcgcccctcagacgagtcggatcctcttggccgctccccgc

Reads alignment and analysis of plate-based full-length Smart-Seq2 dataset: Raw reads were first trimmed by Trimmomatic (version 0.39) and then aligned to GRCm38 (Genome Reference Consortium Mouse Build 38) downloaded from (https://cloud.biohpc.swmed.edu/index.php/s/grcm38_tran/download) using Hisat2 (version 2.1.0). Gene expression matrices for each cell were quantified using featureCounts with GRCm38 transcriptome file version 81. Low quality cells were filtered out using the following criteria: $\geq 500,000$ total reads mapped to genome, ≥ 1500 genes detected in each cell, $\geq 40\%$ of reads mapped to the transcriptome. Count matrix calculated with Reads Per Kilobase of transcript, per Million mapped reads (RPKM) was generated for all the cells passed the filter. A similar analysis pipeline was applied for downstream analysis. To identify the RGC type to which each cell belonged, two methods were used. First, a type predictor was built from the droplet-based dataset (Tran et al., 2019) using the “XGBoost” algorithm. Second, correlation analysis was performed to seek the most similar type for each cell based on the overall gene expression. The two methods yielded consistent results, indicating reliable RGC type identification. To quantify regenerating RGC subclass contribution, numbers arising from the correlation analysis were used.

Measure expression of gene sets: The overall expression of gene sets identified previously (Tran et al., 2019) or from current study were measured using gene set scores. First, genes in the list were filtered to remove those in $< 25\%$ of cells of all types. Then, for each cell, the mean expression value of the genes in the set j ($Exp_{i,j}$) and in the total transcripts (Exp_i) were calculated. Next, the score of gene set j in cell i ($S_{i,j}$) was calculated as $= Exp_{i,j} - Exp_i$. Finally, the averaged score of gene set j in each group was visualized in Figure 3B,H and Figure S4I.

Co-expression gene modules: We used Monocle3 (Cao et al., 2019; Qiu et al., 2017; Trapnell et al., 2014) to examine gene co-expression modules in our scRNA-seq dataset. The dataset was pre-processed using the ‘preprocess_cds’ function (num_dim = 100) by the “PCA” method and dimensionality was reduced using the ‘reduce_dimensions’ function. Batch differences were corrected by the MNN method using the ‘align_cds’ (dimensions

= 100) function and dimension reduction was repeated (Haghverdi et al., 2018). Cells were clustered using the “louvain” method (Levine et al., 2015) using the ‘cluster_cells’ function (k=100) and plotted by ‘UMAP’. Cluster-specific genes were identified using the ‘top_markers’ function. To find gene co-expression modules, we input the resulting cluster-specific genes and used the ‘find_gene_modules’ (resolution = 1e-2). This resulted in 6 gene expression modules (Table S6), which we then plotted for single cells using ‘UMAP’ or by cluster using ‘pheatmap’.

Transcriptional regulatory network analysis using Scenic: To identify transcriptional regulatory networks, we applied the computational method “Scenic” (Aibar et al., 2017; van de Sande et al., 2020) to cells collected at each time point separately using expression matrix of all the genes. The function “SCENICprotocol” was run with Nextflow using the singularity image. The list of TFs, genome ranking databases and motif to transcription factor annotations database for mm10 were downloaded from <https://resources.aertslab.org/cistarget/>. For gene ranks, the 10kb upstream and 10k downstream around the transcription start site were used as search space. Visualization of the result was performed using customized R and Python scripts.

GO-pathway analysis of gene lists: Gene ontology analysis was performed on the DE gene lists generated by group comparisons. Cut offs for inclusion of genes obtained from DE analysis are indicated in the individual tables (S2–S5). Ensemble based annotation package “EnsDb.Mmusculus.v79” and Genome wide annotation for Mouse “org.Mm.eg.db” were used by R package “clusterProfiler” (Yu et al., 2012) to identify the enriched pathways.

QUANTIFICATION AND STATISTICAL ANALYSIS

Retinal whole mounts—RGC density was quantified by immunostaining retina whole mounts with an antibody against RBPMS, a pan RGC marker (Rodriguez et al., 2014). Retinas were examined with epifluorescent illumination. Each quadrant was checked for signs of injection site damage, inflammation, or other damage and areas with obvious damage or inflammation were excluded from further analysis. For imaging, the temporal quadrant was avoided because it has a high density of α alphaRGCs (Bleckert et al., 2014), which, as described in results, are resilient to injury. The entirety of one of the other three quadrants was imaged by a tiled Z-stack scan by confocal microscopy on either a Zeiss 710 or Olympus Fluoview1000 scanning laser confocal microscope. A maximum projection spanning the ganglion cell layer was obtained, and the image background was adjusted using the ‘normalize local contrast’ filter in ImageJ. Quantification of RBPMS density used a semi-automated counting method, as previously described in Tran et al. (2019). Briefly, the processed image was thresholded by the ‘Otsu’ method using Cell Profiler 4.0 (Carpenter et al., 2006) to identify regions-of-interest (ROIs) that demarcated RBPMS+ cells. The resulting ROIs were then exported to a TIFF file and the centroid position of each ROI was determined using the ‘analyze particles’ function in ImageJ and an overlay of the original image, ROI outline, and centroid position was produced. These overlaid images were further analyzed in Matlab to determine the density of RGCs in each quadrant using custom scripts. For each retinal quadrant, the bounding regions of the quadrant were interactively selected by the user, avoiding the quadrant edges, which

can have increased autofluorescence, and areas with minor damage from dissection. Mean densities were calculated as RGCs/mm². Significance was determined by Student's t-test and p-values were FDR adjusted for multiple comparisons.

Retinal sections (CARTPT vs. Gal)—The fluorescent intensity of CART immunostaining and Gal in situ hybridization probe staining were quantified as previously described (Carpenter et al., 2006; Yan et al., 2020). Briefly, three stained sagittal retinal sections were imaged for each condition by confocal microscopy (Zeiss 710) at 40x magnification. Z-stacked images were analyzed in ImageJ. Custom ImageJ macros were used to place circular regions of interest (ROIs; diameter, 3.44 μm) over all cell nuclei/somas that were positive for at least one marker. Fluorescent probe intensity was measured for each marker in each ROI in single Z-slice images. Values were background subtracted using a collection of ROIs negative for both markers. Correlation co-efficient values were calculated in Microsoft Excel and compared to randomized data.

Axon regeneration—The cleared, whole nerve was imaged with a 20X air objective, zoom 1x. From the center of the nerve, 7 single stacks (2μm stack size) were maximum projected to a total volume of 14μm per nerve. After defining the crush site, lines spaced equidistant from each other at 500μm intervals from the crush site to where the longest axon could be detected were introduced for bin-by-bin axon quantification. As described previously (Duan et al., 2015; Park et al., 2008), we quantified the total number of regenerating axons, Σ_{ad} , using the formula $\Sigma_{ad} = \pi r^2 \times [\text{average axons/mm}]/t$, where the total number of axons extending distance d in a nerve having a radius of r was estimated by summing over all sections with thickness t .

For CRISPR-Cas9 mediated KO candidates, maximum projections of Z-stack images were used to capture all regenerated axons. For image analysis, fluorescent intensity profiles along the nerve were generated by the built-in function of ImageJ: Analyze/Plot Profile. To calculate the integral of fluorescent intensity across the entire length of the nerve, a Matlab algorithm was developed (Tian et al., accompanying paper) to quantify the “area under curve” from the plot profile data generated by ImageJ.

Supplementary Material

Refer to Web version on PubMed Central for supplementary material.

ACKNOWLEDGEMENTS

We thank Chen Wang, Yiming Zhang, McKinzie E Arnold and staff members of the Harvard University Bauer Core Facility for technical assistance, Zhiyun Yang and members of the Harvard Catalyst team for support on statistical analysis, and Karthik Shekhar for support in bioinformatic analysis. This work was supported by grants from Wings for Life Spinal Cord Research Foundation to A.J., and NIH grants NS104248-01 to J.R.S., EY029360 to N.T, EY030204-01 to J.R.S and Z.H., EY032181 to F.T. and R01EY021526 and R01EY026939 to Z.H and the Dr. Miriam and Sheldon G. Adelson Medical Research Foundation (to Z.H.) and Gilbert Family Foundation (to Z.H.). Viral cores were supported by the grants from the NIH (HD018655 and P30EY012196).

REFERENCES

- Abe N, and Cavalli V (2008). Nerve injury signaling. *Current Opinion in Neurobiology* 18, 276–283. 10.1016/j.conb.2008.06.005. [PubMed: 18655834]
- Aibar S, González-Blas CB, Moerman T, Huynh-Thu VA, Imrichova H, Hulselmans G, Rambow F, Marine JC, Geurts P, Aerts J, et al. (2017). SCENIC: Single-cell regulatory network inference and clustering. *Nature Methods* 14, 1083–1086. 10.1038/NMETH.4463. [PubMed: 28991892]
- Babon JJ, Kershaw NJ, Murphy JM, Varghese LN, Laktyushin A, Young SN, Lucet IS, Norton RS, and Nicola NA (2012). Suppression of Cytokine Signaling by SOCS3: Characterization of the Mode of Inhibition and the Basis of Its Specificity. *Immunity* 36, 239–250. 10.1016/j.immuni.2011.12.015. [PubMed: 22342841]
- Baskozos G, Sandy-Hindmarch O, Clark AJ, Windsor K, Karlsson P, Weir GA, McDermott LA, Burchall J, Wiberg A, Furniss D, et al. (2020). Molecular and cellular correlates of human nerve regeneration: ADCYAP1/PACAP enhance nerve outgrowth. *Brain* 143, 2009–2026. 10.1093/brain/awaa163. [PubMed: 32651949]
- Baudet ML, Rattray D, Martin BT, and Harvey S (2009). Growth hormone promotes axon growth in the developing nervous system. *Endocrinology* 150, 2758–2766. 10.1210/en.2008-1242. [PubMed: 19213842]
- Benowitz LI, and Popovich PG (2011). Inflammation and axon regeneration. *Current Opinion in Neurology* 24, 577–583. 10.1097/WCO.0b013e32834c208d. [PubMed: 21968547]
- Bleckert A, Schwartz GW, Turner MH, Rieke F, and Wong ROL (2014). Visual Space Is Represented by Nonmatching Topographies of Distinct Mouse Retinal Ganglion Cell Types. *Current Biology* 24, 310–315. 10.1016/J.CUB.2013.12.020. [PubMed: 24440397]
- Bollaerts I, van houcke J, Andries L, de Groef L, and Moons L (2017). Neuroinflammation as Fuel for Axonal Regeneration in the Injured Vertebrate Central Nervous System. *Mediators of Inflammation* 2017, 9478542. 10.1155/2017/9478542. [PubMed: 28203046]
- Bonilla IE, Tanabe K, and Strittmatter SM (2002). Small proline-rich repeat protein 1A is expressed by axotomized neurons and promotes axonal outgrowth. *Journal of Neuroscience* 22, 1303–1315. 10.1523/jneurosci.22-04-01303.2002. [PubMed: 11850458]
- Bray ER, Yungheer BJ, Levay K, Ribeiro M, Dvoryanchikov G, Ayupe AC, Thakor K, Marks V, Randolph M, Danzi MC, et al. (2019). Thrombospondin-1 Mediates Axon Regeneration in Retinal Ganglion Cells. *Neuron* 103, 642–657.e7. 10.1016/j.neuron.2019.05.044. [PubMed: 31255486]
- Cai D, Yingjing S, de Bellard ME, Tang S, and Filbin MT (1999). Prior Exposure to Neurotrophins Blocks Inhibition of Axonal Regeneration by MAG and Myelin via a cAMP-Dependent Mechanism. *Neuron* 22, 89–101. 10.1016/S0896-6273(00)80681-9. [PubMed: 10027292]
- Cao J, Spielmann M, Qiu X, Huang X, Ibrahim DM, Hill AJ, Zhang F, Mundlos S, Christiansen L, Steemers FJ, et al. (2019). The single-cell transcriptional landscape of mammalian organogenesis. *Nature* 566, 496–502. 10.1038/s41586-019-0969-x. [PubMed: 30787437]
- Carpenter AE, Jones TR, Lamprecht MR, Clarke C, Kang IH, Friman O, Guertin DA, Chang JH, Lindquist RA, Moffat J, et al. (2006). CellProfiler: Image analysis software for identifying and quantifying cell phenotypes. *Genome Biology* 7. 10.1186/gb-2006-7-10-r100.
- Chandran V, Coppola G, Nawabi H, Omura T, Versano R, Huebner EA, Zhang A, Costigan M, Yekkirala A, Barrett L, et al. (2016). A Systems-Level Analysis of the Peripheral Nerve Intrinsic Axonal Growth Program. *Neuron* 89, 956–970. 10.1016/J.NEURON.2016.01.034. [PubMed: 26898779]
- Cherry TJ, Wang S, Bormuth I, Schwab M, Olson J, and Cepko CL (2011). NeuroD factors regulate cell fate and neurite stratification in the developing retina. *Journal of Neuroscience* 31, 7365–7379. 10.1523/JNEUROSCI.2555-10.2011. [PubMed: 21593321]
- Crocker BA, Kiu H, and Nicholson SE (2008). SOCS regulation of the JAK/STAT signalling pathway. *Seminars in Cell and Developmental Biology* 19, 414–422. 10.1016/j.semcdb.2008.07.010. [PubMed: 18708154]
- Danilov CA, and Steward O (2015). Conditional genetic deletion of PTEN after a spinal cord injury enhances regenerative growth of CST axons and motor function recovery in mice. *Experimental Neurology* 266, 147–160. 10.1016/J.EXPNEUROL.2015.02.012. [PubMed: 25704959]

- Du K, Zheng S, Zhang Q, Li S, Gao X, Wang J, Jiang L, and Liu K (2015). Pten Deletion Promotes Regrowth of Corticospinal Tract Axons 1 Year after Spinal Cord Injury. *The Journal of Neuroscience* 35, 9754 LP–9763. 10.1523/JNEUROSCI.3637-14.2015. [PubMed: 26134657]
- Duan X, Qiao M, Bei F, Kim IJ, He Z, and Sanes JR (2015). Subtype-Specific regeneration of retinal ganglion cells following axotomy: Effects of osteopontin and mtor signaling. *Neuron* 85, 1244–1256. 10.1016/j.neuron.2015.02.017. [PubMed: 25754821]
- Enes J, Langwieser N, Ruschel J, Carballosa-Gonzalez MM, Klug A, Traut MH, Ylera B, Tahirovic S, Hofmann F, Stein V, et al. (2010). Electrical activity suppresses axon growth through Cav1.2 channels in adult primary sensory neurons. *Current Biology* 20, 1154–1164. 10.1016/j.cub.2010.05.055. [PubMed: 20579880]
- Feng G, Mellor RH, Bernstein M, Keller-Peck C, Nguyen QT, Wallace M, Nerbonne JM, Lichtman JW, and Sanes JR (2000). Imaging Neuronal Subsets in Transgenic Mice Expressing Multiple Spectral Variants of GFP. *Neuron* 28, 41–51. 10.1016/S0896-6273(00)00084-2. [PubMed: 11086982]
- Fudalej E, Justyniarska M, Kasarek K, Dziedziak J, Szaflik JP, and Cudnoch-Jędrzejewska A (2021). Neuroprotective Factors of the Retina and Their Role in Promoting Survival of Retinal Ganglion Cells: A Review. *Ophthalmic Research* 64, 345–355. 10.1159/000514441. [PubMed: 33454713]
- Gao Y, Banik DD, Muna MM, Roberts SGE, and Medler KF (2019). The WT1-BASP1 complex is required to maintain the differentiated state of taste receptor cells. *Life Science Alliance* 2, 1–9. 10.26508/lsa.201800287.
- Gentleman RC, Carey VJ, Bates DM, Bolstad B, Dettling M, Dudoit S, Ellis B, Gautier L, Ge Y, Gentry J, et al. (2004). Bioconductor: open software development for computational biology and bioinformatics. *Genome Biol* 5. 10.1186/gb-2004-5-10-r80.
- Haghverdi L, Lun ATL, Morgan MD, and Marioni JC (2018). Batch effects in single-cell RNA-sequencing data are corrected by matching mutual nearest neighbors. *Nature Biotechnology* 36, 421–427. 10.1038/nbt.4091.
- Hannila SS, and Filbin MT (2008). The role of cyclic AMP signaling in promoting axonal regeneration after spinal cord injury. *Experimental Neurology* 209, 321–332. 10.1016/J.EXPNEUROL.2007.06.020. [PubMed: 17720160]
- Hao Y, Hao S, Andersen-Nissen E, Mauck WM, Zheng S, Butler A, Lee MJ, Wilk AJ, Darby C, Zager M, et al. (2021). Integrated analysis of multimodal single-cell data. *Cell* 184, 3573–3587.e29. 10.1016/J.CELL.2021.04.048. [PubMed: 34062119]
- Hartl M, and Schneider R (2019). A unique family of neuronal signaling proteins implicated in oncogenesis and tumor suppression. *Frontiers in Oncology* 9, 1–13. 10.3389/fonc.2019.00289. [PubMed: 30761267]
- He Z, and Jin Y (2016). Intrinsic Control of Axon Regeneration. *Neuron* 90, 437–451. 10.1016/j.neuron.2016.04.022. [PubMed: 27151637]
- Hellström M, Pollett MA, and Harvey AR (2011). Post-injury delivery of rAAV2-CNTF combined with short-term pharmacotherapy is neuroprotective and promotes extensive axonal regeneration after optic nerve trauma. *Journal of Neurotrauma* 28, 2475–2483. 10.1089/neu.2011.1928. [PubMed: 21861632]
- Hill R, and Wu H (2009). PTEN, stem cells, and cancer stem cells. *Journal of Biological Chemistry* 284, 11755–11759. 10.1074/jbc.R800071200. [PubMed: 19117948]
- Hilton BJ, and Bradke F (2017). Can injured adult CNS axons regenerate by recapitulating development? *Development* 144, 3417–3429. 10.1242/dev.148312. [PubMed: 28974639]
- Hilton BJ, Husch A, Schaffran B, Lin T, Burnside ER, Dupraz S, Schelski M, Kim J, Müller JA, Schoch S, et al. (2022). An active vesicle priming machinery suppresses axon regeneration upon adult CNS injury. *Neuron* 110, 51–69.e7. 10.1016/j.neuron.2021.10.007. [PubMed: 34706221]
- Holmes FE, Mahoney S, King VR, Bacon A, Kerr NCH, Pachnis V, Curtis R, Priestley J v, and Wynick, D. (2000). Targeted disruption of the galanin gene reduces the number of sensory neurons and their regenerative capacity. *Proc Natl Acad Sci U S A* 97, 11563–11568. 10.1073/pnas.210221897. [PubMed: 11016970]
- Hu Y, Park KK, Yang L, Wei X, Yang Q, Cho KS, Thielen P, Lee AH, Cartoni R, Glimcher LH, et al. (2012). Differential Effects of Unfolded Protein Response Pathways on Axon Injury-

- Induced Death of Retinal Ganglion Cells. *Neuron* 73, 445–452. 10.1016/J.NEURON.2011.11.026. [PubMed: 22325198]
- Huff V (2011). Wilms' tumours: About tumour suppressor genes, an oncogene and a chameleon gene. *Nature Reviews Cancer* 11, 111–121. 10.1038/nrc3002. [PubMed: 21248786]
- Hung SSC, Chrysostomou V, Li F, Lim JKH, Wang JH, Powell JE, Tu L, Daniszewski M, Lo C, Wong RC, et al. (2016). AAV-Mediated CRISPR/Cas Gene Editing of Retinal Cells in Vivo. *Investigative Ophthalmology and Visual Science* 57, 3470–3476. 10.1167/iovs.16-19316. [PubMed: 27367513]
- Jankowski MP, McIlwrath SL, Jing X, Cornuet PK, Salerno KM, Koerber HR, and Albers KM (2009). Sox11 transcription factor modulates peripheral nerve regeneration in adult mice. *Brain Research* 1256, 43–54. 10.1016/j.brainres.2008.12.032. [PubMed: 19133245]
- Jaworski J, and Sheng M (2006). The Growing Role of mTOR in Neuronal Development and Plasticity. *Molecular Neurobiology* 205.
- Katic J, Loers G, Kleene R, Karl N, Schmidt C, Buck F, Zmijewski JW, Jakovcevski I, Preissner KT, and Schachner M (2014). Interaction of the cell adhesion molecule CHL1 with vitronectin, Integrins, And the plasminogen activator inhibitor-2 promotes CHL1-induced neurite outgrowth and neuronal migration. *Journal of Neuroscience* 34, 14606–14623. 10.1523/JNEUROSCI.3280-13.2014. [PubMed: 25355214]
- Kershaw NJ, Murphy JM, Liao NPD, Varghese LN, Laktyushin A, Whitlock EL, Lucet IS, Nicola NA, and Babon JJ (2013). SOCS3 binds specific receptor-JAK complexes to control cytokine signaling by direct kinase inhibition. *Nature Structural and Molecular Biology* 20, 469–476. 10.1038/nsmb.2519.
- Kingston R, Amin D, Misra S, Gross JM, and Kuwajima T (2021). Serotonin transporter-mediated molecular axis regulates regional retinal ganglion cell vulnerability and axon regeneration after nerve injury. *PLOS Genetics* 17, e1009885. [PubMed: 34735454]
- Kole C, Brommer B, Nakaya N, Sengupta M, Bonet-Ponce L, Zhao T, Wang C, Li W, He Z, and Tomarev S (2020). Activating transcription factor 3 (ATF3) protects retinal ganglion cells and promotes functional preservation after optic nerve crush. *Investigative Ophthalmology and Visual Science* 61. 10.1167/iovs.61.2.31.
- Latremoliere A, Cheng L, DeLisle M, Wu C, Chew S, Hutchinson EB, Sheridan A, Alexandre C, Latremoliere F, Sheu SH, et al. (2018). Neuronal-Specific TUBB3 Is Not Required for Normal Neuronal Function but Is Essential for Timely Axon Regeneration. *Cell Reports* 24, 1865–1879.e9. 10.1016/J.CELREP.2018.07.029. [PubMed: 30110642]
- Léveillé F, Papadia S, Fricker M, Bell KFS, Soriano FX, Martel MA, Puddifoot C, Habel M, Wyllie DJ, Ikonomidou C, et al. (2010). Suppression of the intrinsic apoptosis pathway by synaptic activity. *Journal of Neuroscience* 30, 2623–2635. 10.1523/JNEUROSCI.5115-09.2010. [PubMed: 20164347]
- Levine JH, Simonds EF, Bendall SC, Davis KL, Amir EAD, Tadmor MD, Litvin O, Fienberg HG, Jager A, Zunder ER, et al. (2015). Data-Driven Phenotypic Dissection of AML Reveals Progenitor-like Cells that Correlate with Prognosis. *Cell* 162, 184–197. 10.1016/j.cell.2015.05.047. [PubMed: 26095251]
- Li S, Yang C, Zhang L, Gao X, Wang X, Liu W, Wang Y, Jiang S, Wong YH, Zhang Y, et al. (2016). Promoting axon regeneration in the adult CNS by modulation of the melanopsin/GPCR signaling. *Proceedings of the National Academy of Sciences* 113, 1937 LP–1942. 10.1073/pnas.1523645113.
- Li Y, He X, Kawaguchi R, Zhang Y, Wang Q, Monavarfeshani A, Yang Z, Chen B, Shi Z, Meng H, et al. (2020). Microglia-organized scar-free spinal cord repair in neonatal mice. *Nature* 587, 613–618. 10.1038/s41586-020-2795-6. [PubMed: 33029008]
- Lim J-HA, Stafford BK, Nguyen PL, Lien B. v, Wang C, Zukor K, He Z, and Huberman AD (2016). Neural activity promotes long-distance, target-specific regeneration of adult retinal axons. *Nature Neuroscience* 19, 1073–1084. 10.1038/nn.4340. [PubMed: 27399843]
- Loeb DM (2006). WT1 Influences Apoptosis Through Transcriptional Regulation of Bcl-2 Family Members. *Cell Cycle* 5, 1249–1253. 10.4161/cc.5.12.2807. [PubMed: 16760668]
- Luo X, and Park KK (2012). Neuron-Intrinsic Inhibitors of Axon Regeneration: PTEN and SOCS3. *International Review of Neurobiology* 105, 141–173. 10.1016/B978-0-12-398309-1.00008-1. [PubMed: 23206599]

- Luo X, Salgueiro Y, Beckerman SR, Lemmon VP, Tsoulfas P, and Park KK (2013). Three-dimensional evaluation of retinal ganglion cell axon regeneration and pathfinding in whole mouse tissue after injury. *Experimental Neurology* 247, 653–662. 10.1016/J.EXPNEUROL.2013.03.001. [PubMed: 23510761]
- Ma TC, Barco A, Ratan RR, and Willis DE (2014). cAMP-responsive element-binding protein (CREB) and cAMP co-regulate activator protein 1 (AP1)-dependent regeneration-associated gene expression and neurite growth. *Journal of Biological Chemistry* 289, 32914–32925. 10.1074/jbc.M114.582460. [PubMed: 25296755]
- Manning BD, and Cantley LC (2007). AKT/PKB Signaling: Navigating Downstream. *Cell* 129, 1261–1274. 10.1016/j.cell.2007.06.009. [PubMed: 17604717]
- Marquardt T, Ashery-Padan R, Andrejewski N, Scardigli R, Guillemot F, and Gruss P (2001). Pax6 Is Required for the Multipotent State of Retinal Progenitor Cells. *Cell* 105, 43–55. 10.1016/S0092-8674(01)00295-1. [PubMed: 11301001]
- Morgan-Warren PJ, Berry M, Ahmed Z, Scott RAH, and Logan A (2013). Exploiting mTOR Signaling: A Novel Translatable Treatment Strategy for Traumatic Optic Neuropathy? *Investigative Ophthalmology & Visual Science* 54, 6903–6916. 10.1167/iovs.13-12803. [PubMed: 24154996]
- Müller A, Hauk TG, and Fischer D (2007). Astrocyte-derived CNTF switches mature RGCs to a regenerative state following inflammatory stimulation. *Brain* 130, 3308–3320. 10.1093/brain/awm257. [PubMed: 17971355]
- Neumann S, and Woolf CJ (1999). Regeneration of dorsal column fibers into and beyond the lesion site following adult spinal cord injury. *Neuron* 23, 83–91. 10.1016/S0896-6273(00)80755-2. [PubMed: 10402195]
- Nieuwenhuis B, and Eva R (2022). Promoting axon regeneration in the central nervous system by increasing PI3-kinase signaling. *Neural Regen Res* 17, 1172–1182. 10.4103/1673-5374.327324. [PubMed: 34782551]
- Palkovits M (1995). Neuropeptide messenger plasticity in the CNS neurons following axotomy. *Molecular Neurobiology* 10, 91–103. 10.1007/BF02740669. [PubMed: 7576312]
- Park KK, Liu K, Hu Y, Smith PD, Wang C, Cai B, Xu B, Connolly L, Kramvis I, Sahin M, et al. (2008). Promoting axon regeneration in the adult CNS by modulation of the PTEN/mTOR pathway. *Science* (1979) 322, 963–966. 10.1126/science.1161566.
- Pernet V, Joly S, Dalkara D, Jordi N, Schwarz O, Christ F, Schaffer D. v., Flannery JG, and Schwab ME (2013). Long-distance axonal regeneration induced by CNTF gene transfer is impaired by axonal misguidance in the injured adult optic nerve. *Neurobiology of Disease* 51, 202–213. 10.1016/j.nbd.2012.11.011. [PubMed: 23194670]
- Peterson WM, Wang Q, Tzekova R, and Wiegand SJ (2000). Ciliary neurotrophic factor and stress stimuli activate the Jak-STAT pathway in retinal neurons and glia. *Journal of Neuroscience* 20, 4081–4090. 10.1523/jneurosci.20-11-04081.2000. [PubMed: 10818143]
- Picelli S, Faridani OR, Björklund ÅK, Winberg G, Sagasser S, and Sandberg R (2014). Full-length RNA-seq from single cells using Smart-seq2. *Nature Protocols* 9, 171–181. 10.1038/nprot.2014.006. [PubMed: 24385147]
- Planchon SM, Waite KA, and Eng C (2008). The nuclear affairs of PTEN. *Journal of Cell Science* 121, 249–253. 10.1242/jcs.022459. [PubMed: 18216329]
- Poplawski GHD, Kawaguchi R, van Niekerk E, Lu P, Mehta N, Canete P, Lie R, Dragatsis I, Meves JM, Zheng B, et al. (2020). Injured adult neurons regress to an embryonic transcriptional growth state. *Nature* 581, 77–82. 10.1038/s41586-020-2200-5. [PubMed: 32376949]
- Qiu X, Mao Q, Tang Y, Wang L, Chawla R, Pliner HA, and Trapnell C (2017). Reversed graph embedding resolves complex single-cell trajectories. *Nature Methods* 14, 979–982. 10.1038/nmeth.4402. [PubMed: 28825705]
- Ramon y Cajal S (1928). Degeneration and regeneration of the nervous system.
- Rauscher FJ (1993). The WT1 Wilms tumor gene product: a developmentally regulated transcription factor in the kidney that functions as a tumor suppressor. *The FASEB Journal* 7, 896–903. 10.1096/fasebj.7.10.8393820. [PubMed: 8393820]

- Renier N, Wu Z, Simon DJ, Yang J, Ariel P, and Tessier-Lavigne M (2014). IDISCO: A simple, rapid method to immunolabel large tissue samples for volume imaging. *Cell* 159, 896–910. 10.1016/j.cell.2014.10.010. [PubMed: 25417164]
- Renthal W, Tochitsky I, Yang L, Cheng YC, Li E, Kawaguchi R, Geschwind DH, and Woolf CJ (2020). Transcriptional Reprogramming of Distinct Peripheral Sensory Neuron Subtypes after Axonal Injury. *Neuron* 108, 128–144.e9. 10.1016/j.neuron.2020.07.026. [PubMed: 32810432]
- Richardson PM (1994). Ciliary neurotrophic factor: A review. *Pharmacology and Therapeutics* 63, 187–198. 10.1016/0163-7258(94)90045-0. [PubMed: 7809179]
- Richardson PM, and Issa VMK (1984). Peripheral injury enhances central regeneration of primary sensory neurones. *Nature* 309, 791–793. 10.1038/309791a0. [PubMed: 6204205]
- Richner M, Ulrichsen M, Elmegaard SL, Dieu R, Pallesen LT, and Vaegter CB (2014). Peripheral Nerve Injury Modulates Neurotrophin Signaling in the Peripheral and Central Nervous System. *Molecular Neurobiology* 50, 945–970. 10.1007/s12035-014-8706-9. [PubMed: 24752592]
- Rodriguez AR, de Sevilla Müller LP, and Brecha NC (2014). The RNA binding protein RBPMS is a selective marker of ganglion cells in the mammalian retina. *Journal of Comparative Neurology* 522, 1411–1443. 10.1002/cne.23521. [PubMed: 24318667]
- Romaniello R, Tonelli A, Arrigoni F, Baschiroto C, Triulzi F, Bresolin N, Bassi MT, and Borgatti R (2012). A novel mutation in the β -tubulin gene TUBB2B associated with complex malformation of cortical development and deficits in axonal guidance. *Developmental Medicine and Child Neurology* 54, 765–769. 10.1111/j.1469-8749.2012.04316.x. [PubMed: 22591407]
- Rubin CI, and Atweh GF (2004). The role of stathmin in the regulation of the cell cycle. *Journal of Cellular Biochemistry* 93, 242–250. 10.1002/jcb.20187. [PubMed: 15368352]
- van de Sande B, Flerin C, Davie K, de Waegeneer M, Hulselmans G, Aibar S, Seurinck R, Saelens W, Cannoodt R, Rouchon Q, et al. (2020). A scalable SCENIC workflow for single-cell gene regulatory network analysis. *Nature Protocols* 15, 2247–2276. 10.1038/s41596-020-0336-2. [PubMed: 32561888]
- Sanders EJ, Parker E, Arámburo C, and Harvey S (2005). Retinal growth hormone is an anti-apoptotic factor in embryonic retinal ganglion cell differentiation. *Experimental Eye Research* 81, 551–560. 10.1016/j.exer.2005.03.013. [PubMed: 15913606]
- Schindelin J, Arganda-Carreras I, Frise E, Kaynig V, Longair M, Pietzsch T, Preibisch S, Rueden C, Saalfeld S, Schmid B, et al. (2012). Fiji: An open-source platform for biological-image analysis. *Nature Methods* 9, 676–682. 10.1038/nmeth.2019. [PubMed: 22743772]
- Schwartz M, and Raposo C (2014). Protective autoimmunity: A unifying model for the immune network involved in CNS repair. *Neuroscientist* 20, 343–358. 10.1177/1073858413516799. [PubMed: 24395337]
- Smith PD, Sun F, Park KK, Cai B, Wang C, Kuwako K, Martinez-Carrasco I, Connolly L, and He Z (2009). SOCS3 Deletion Promotes Optic Nerve Regeneration In Vivo. *Neuron* 64, 617–623. 10.1016/j.neuron.2009.11.021. [PubMed: 20005819]
- Sun F, Park KK, Belin S, Wang D, Lu T, Chen G, Zhang K, Yeung C, Feng G, Yankner BA, et al. (2011). Sustained axon regeneration induced by co-deletion of PTEN and SOCS3. *Nature* 480, 372–375. 10.1038/nature10594. [PubMed: 22056987]
- Sun LO, Brady CM, Cahill H, Al-Khindi T, Sakuta H, Dhande OS, Noda M, Huberman AD, Nathans J, and Kolodkin AL (2015). Functional Assembly of Accessory Optic System Circuitry Critical for Compensatory Eye Movements. *Neuron* 86, 971–984. 10.1016/j.neuron.2015.03.064. [PubMed: 25959730]
- Suter TACS, Blagburn S. v., Fisher SE, Anderson-Keightly HM, D’Elia KP, and Jaworski A (2020). TAG-1 Multifunctionality Coordinates Neuronal Migration, Axon Guidance, and Fasciculation. *Cell Reports* 30, 1164–1177.e7. 10.1016/j.celrep.2019.12.085. [PubMed: 31995756]
- Syc-Mazurek SB, Fernandes KA, Wilson MP, Shrager P, and Libby RT (2017). Together JUN and DDIT3 (CHOP) control retinal ganglion cell death after axonal injury. *Molecular Neurodegeneration* 12, 71. 10.1186/s13024-017-0214-8. [PubMed: 28969695]
- Tedeschi A, Dupraz S, Laskowski CJ, Xue J, Ulas T, Beyer M, Schultze JL, and Bradke F (2016). The Calcium Channel Subunit Alpha2delta2 Suppresses Axon Regeneration in the Adult CNS. *Neuron* 92, 419–434. 10.1016/j.neuron.2016.09.026. [PubMed: 27720483]

- Tian F, Cheng Y, Zhou S, Wang C, Monavarfeshani A, Gao K, Jiang W, Kawaguchi R, Wang Q, Tang M, Donahue R, Meng H, Zhang Y, Jacobi A, Yan W, Yan Y, Yin J, Cai X, Yang Z, Hegarty S, Stanicka J, Dmitriev P, Taub D, Zhu J, Woolf CJ, Sanes JR, Geschwind DH and He Z. Core Transcription Programs Controlling Injury-Induced Neurodegeneration of Retinal Ganglion Cells (companion paper).
- Tran NM, Shekhar K, Whitney IE, Jacobi A, Benhar I, Hong G, Yan W, Adiconis X, Arnold ME, Lee JM, et al. (2019). Single-Cell Profiles of Retinal Ganglion Cells Differing in Resilience to Injury Reveal Neuroprotective Genes. *Neuron* 104, 1039–1055.e12. 10.1016/j.neuron.2019.11.006. [PubMed: 31784286]
- Trapnell C, Cacchiarelli D, Grimsby J, Pokharel P, Li S, Morse M, Lennon NJ, Livak KJ, Mikkelsen TS, and Rinn JL (2014). The dynamics and regulators of cell fate decisions are revealed by pseudotemporal ordering of single cells. *Nature Biotechnology* 32, 381–386. 10.1038/nbt.2859.
- Wagner KD, Wagner N, Vidal VPI, Schley G, Wilhelm D, Schedl A, Englert C, and Scholz H (2002). The Wilms' tumor gene *Wt1* is required for normal development of the retina. *EMBO Journal* 21, 1398–1405. 10.1093/emboj/21.6.1398. [PubMed: 11889045]
- Wang Z, Mehra V, Simpson MT, Maunze B, Chakraborty A, Holan L, Eastwood E, Blackmore MG, and Venkatesh I (2018). KLF6 and STAT3 co-occupy regulatory DNA and functionally synergize to promote axon growth in CNS neurons OPEN. *Scientific Reports* | 8, 12565. 10.1038/s41598-018-31101-5. [PubMed: 30135567]
- Williams MR, De-Spenza T, Li M, Gullidge AT, and Luikart BW (2015). Hyperactivity of newborn pten knock-out neurons results from increased excitatory synaptic drive. *Journal of Neuroscience* 35, 943–959. 10.1523/JNEUROSCI.3144-14.2015. [PubMed: 25609613]
- Williams PR, Benowitz LI, Goldberg JL, and He Z (2020). Axon Regeneration in the Mammalian Optic Nerve. *Annual Review of Vision Science* 6, 195–213. 10.1146/annurev-vision-022720-094953.
- Winter CC, He Z, and Jacobi A (2021). Axon Regeneration: A Subcellular Extension in Multiple Dimensions. *Cold Spring Harbor Perspectives in Biology* a040923. 10.1101/cshperspect.a040923.
- Xie L, Yin Y, and Benowitz L (2021). Chemokine CCL5 promotes robust optic nerve regeneration and mediates many of the effects of CNTF gene therapy. *Proceedings of the National Academy of Sciences* 118, e2017282118. 10.1073/pnas.2017282118.
- Yan W, Laboulaye MA, Tran NM, Whitney IE, Benhar I, and Sanes JR (2020). Mouse Retinal Cell Atlas: Molecular Identification of over Sixty Amacrine Cell Types. *The Journal of Neuroscience* 40, 5177 LP–5195. 10.1523/JNEUROSCI.0471-20.2020. [PubMed: 32457074]
- Yang L, Han Y, Saurez Saiz F, and Minden MD (2007). A tumor suppressor and oncogene: The *WT1* story. *Leukemia* 21, 868–876. 10.1038/sj.leu.2404624. [PubMed: 17361230]
- Yang SG, Li CP, Peng XQ, Teng ZQ, Liu CM, and Zhou FQ (2020). Strategies to Promote Long-Distance Optic Nerve Regeneration. *Frontiers in Cellular Neuroscience* 14. 10.3389/fncel.2020.00119.
- Yu C-F, Peng W-M, Schlee M, Barchet W, Eis-Hübinger AM, Kolanus W, Geyer M, Schmitt S, Steinhagen F, Oldenburg J, et al. (2018). SOCS1 and SOCS3 Target IRF7 Degradation To Suppress TLR7-Mediated Type I IFN Production of Human Plasmacytoid Dendritic Cells. *The Journal of Immunology* 200, 4024–4035. 10.4049/jimmunol.1700510. [PubMed: 29712772]
- Yu G, Wang LG, Han Y, and He QY (2012). ClusterProfiler: An R package for comparing biological themes among gene clusters. *OMICS A Journal of Integrative Biology* 16, 284–287. 10.1089/omi.2011.0118. [PubMed: 22455463]
- Yuan H, Xu S, Wang Y, Xu H, Wang C, Zhu Q, Yang RK, Chen X, Yang PC, and Shi X (2010). Corticotrophin-releasing hormone (CRH) facilitates axon outgrowth. *Spinal Cord* 48, 850–856. 10.1038/sc.2010.47. [PubMed: 20458328]
- Zhang Y, Williams PR, Jacobi A, Wang C, Goel A, Hirano AA, Brecha NC, Kerschensteiner D, and He Z (2019). Elevating Growth Factor Responsiveness and Axon Regeneration by Modulating Presynaptic Inputs. *Neuron* 103, 39–51.e5. 10.1016/j.neuron.2019.04.033. [PubMed: 31122676]
- Zheng GXY, Terry JM, Belgrader P, Ryvkin P, Bent ZW, Wilson R, Ziraldo SB, Wheeler TD, McDermott GP, Zhu J, et al. (2017). Massively parallel digital transcriptional profiling of single cells. *Nature Communications* 8. 10.1038/ncomms14049.

van Zyl T, Yan W, McAdams A, Peng Y-R, Shekhar K, Regev A, Juric D, and Sanes JR (2020). Cell atlas of aqueous humor outflow pathways in eyes of humans and four model species provides insight into glaucoma pathogenesis. *Proceedings of the National Academy of Sciences* 117, 10339 LP–10349. [10.1073/pnas.2001250117](https://doi.org/10.1073/pnas.2001250117).

Author Manuscript

Author Manuscript

Author Manuscript

Author Manuscript

Highlights:

- Activating mTOR and JAK/STAT signaling promotes neuronal survival and regeneration
- Single cell RNAseq reveals transcriptional programs regulated by these interventions
- Distinct gene expression modules correlate with apoptosis, survival and regeneration
- Overexpression of regeneration module genes promotes both survival and regeneration

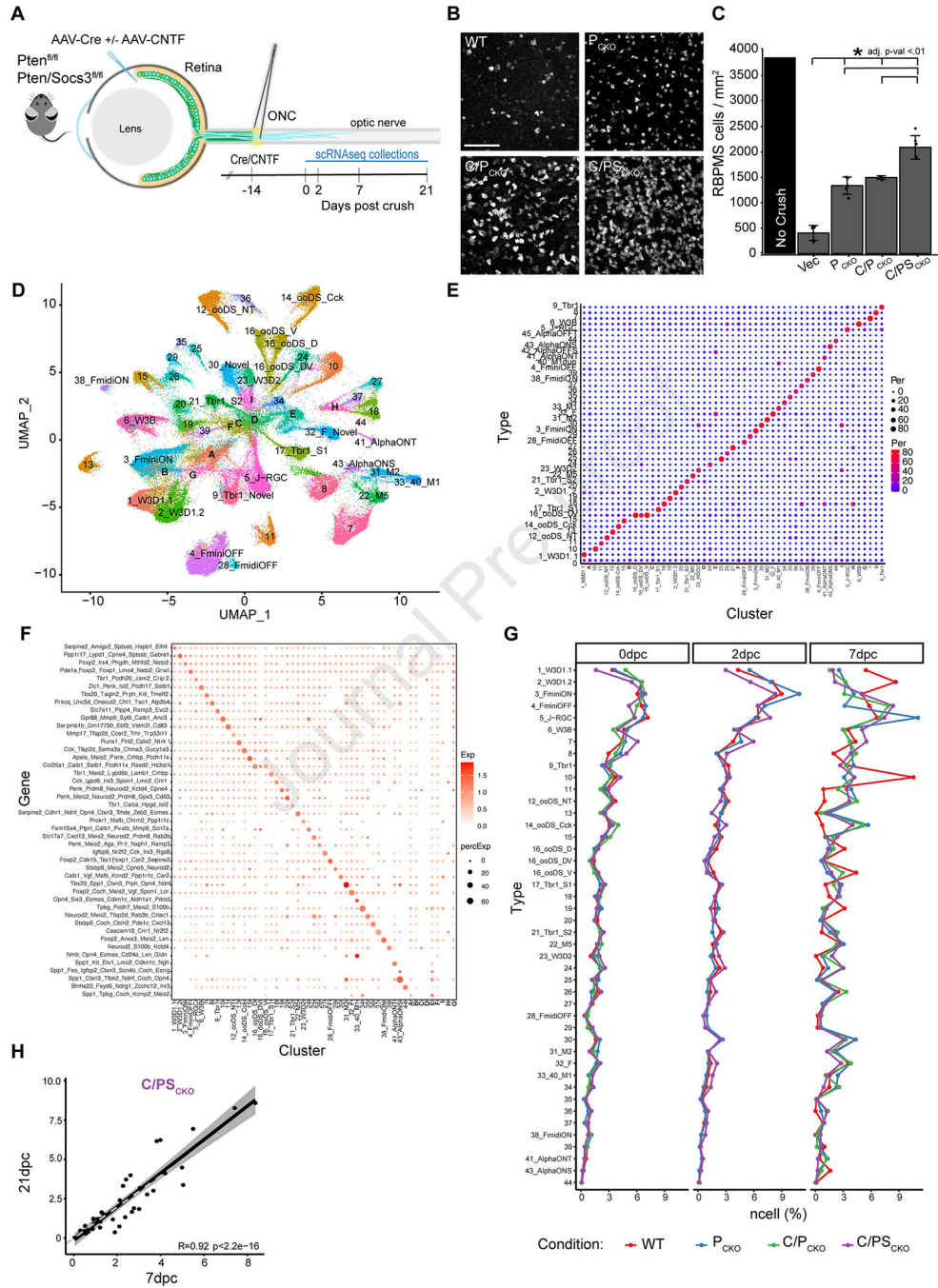


Figure 1: Interventions preserve type identity and increase survival of most RGC types after ONC

A) AAV2-Cre was injected into the vitreous body of $PTEN^{f/f}$ (P_{CKO}) or $Pten^{f/f}Socs3^{f/f}$ (PS_{CKO}) mice to delete the floxed genes 2 weeks before crushing the optic nerve (ONC). AAV2 encoding ciliary neurotrophic factor (CNTF) was co-injected as indicated (C/P_{CKO} or C/PS_{CKO}). RGCs were collected for scRNA-seq at indicated times thereafter.

B) Immunohistochemistry in retinal whole-mounts for the pan-RGC marker, RBPMS, shows increased survival of RGCs at 21dpc following P_{CKO} , C/P_{CKO} and C/PS_{CKO} . Scale bar = $100\mu\text{m}$

C) RGC density (RBPMS⁺/mm² cells, *adjusted p-value <0.01) at 21dpc compared to uncrushed control, measured from images such as those in **B**.

D) scRNA-Seq data from all RGCs analyzed in this study displayed as a UMAP. Numbers indicate RGC ‘Novel ‘types as defined in the atlas presented in Tran, et al. (2019). Letters (A-G) show clusters that could not be assigned to a type.

E) Comparison of cell type mapping in the current dataset to the RGC atlas from Tran et al., (2019) shown as a confusion matrix. Dot sizes and colors represent the percentage of cells in each cluster on the x-axis that match the atlas types on the y-axis.

F) Expression of gene marker combinations from the control RGC atlas in the current dataset. Color of the dot represents the average expression of the gene marker combination, and the dot size represents the proportion of cells expressing these markers.

G) Proportion of types in WT and each intervention at 0, 2 and 7dpc.

H) Scatterplot showing correspondence ($R_{\text{Pearson}} = 0.92$) between frequencies of C/PS_{CKO} RGCs of at 7 and 21dpc. Each dot shows one RGC type. The dark line shows best fit with confidence interval indicated in grey.

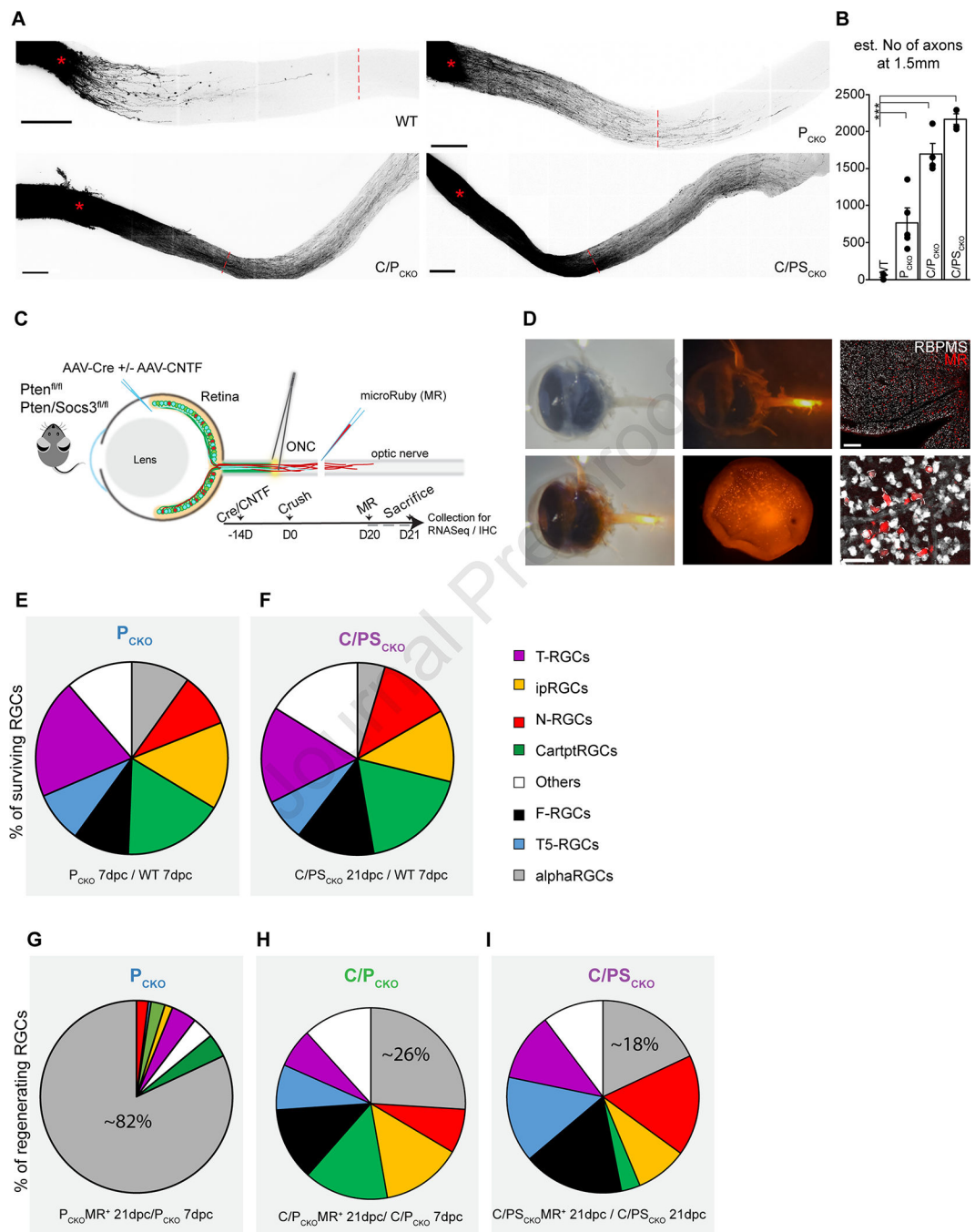


Figure 2: Type-independent axon regeneration in C/PSCKO

A) Maximum projections through cleared optic nerves showing anterograde-labeled RGC axons at 21dpc following injection of AAVs encoding Cre and/or CNTF into *Pten^{fl/fl}* or *Pten^{fl/fl} Socs3^{fl/fl}* mice. An empty vector was injected into WT mice. Scale bar: 250µm; asterisk = crush site; red dashed lines are 1.5mm from crush site.

B) Estimated numbers of regenerating axons 1.5mm distal to injury site at 21dpc, from images such as those shown in **A**. Error bar: SEM; p value by Kruskal – Wallis test and

Bonferroni's post hoc: *** 0.001. Vector n = 7, P_{CKO} n = 5, C/P_{CKO} n = 4, C/PS_{CKO} n = 4.

C) Protocol for retrograde labeling of regenerating RGCs for SS2 collection. 5% Dextran micro-Ruby (MR) was injected into the nerve stump at ~1mm distal to ONC at 20dpc.

D) Eyes collected 21dpc. Left and upper middle panels show fluorescence of injected MR in nerve stump. Lower middle panel shows retrogradely labeled RGCs in a dissected C/PS_{CKO} retina. Right panels from retina as in D but labeled with anti-RBPMS (pan-RGC marker in grey). Dashed lines outline MR⁺ RGCs. Scalebar = 500µm (top), 50µm (bottom).

E) and **F)** Proportions of surviving RGCs by subclass in P_{CKO} (**E**) and C/PS_{CKO} (**F**) among RGCs collected by the 10x Genomics platform. All subclasses are present among surviving RGCs.

G - H) Proportions of regenerating RGCs (MR⁺) among retrograde-labeled RGCs collected by SS2 shown by subclass in P_{CKO} (**G**), C/P_{CKO} (**H**) and C/PS_{CKO} (**I**).

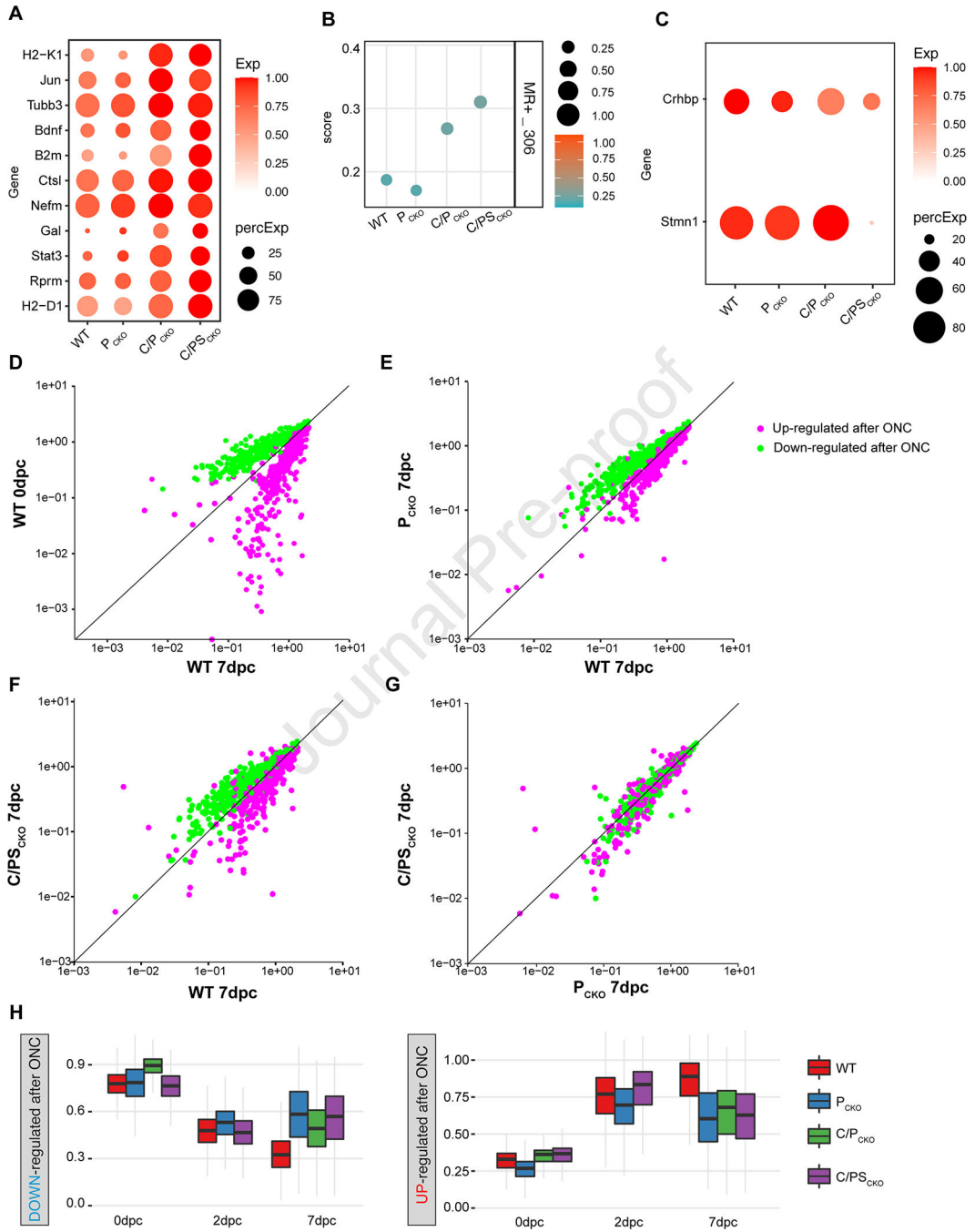


Figure 3: Injury independent effects and mitigation of injury response induced by interventions
A) Dotplot showing genes upregulated in C/P_{CKO} and C/PS_{CKO} compared to WT and P_{CKO} prior to injury (0dpc, 2 weeks after AAV injection).
B) “Composite RAG score” (defined in text), compiled from 306 genes selectively expressed in regenerating (MR⁺) C/PS_{CKO} RGCs.
C) Dotplot showing *Crhbp* and *Stmn1* downregulation in C/PS_{CKO} prior to injury.
D-G) Scatterplots showing expression level in current dataset of 771 genes identified as upregulated (pink) or downregulated (green) after ONC (0.5–14dpc) in a previous study

(Tran et al., 2019). Responses in current data (WT 7dpc vs 0dpc) are similar to those in Tran et al., showing reproducibility (**D**). In P_{CKO} (**E**) or C/PS_{CKO} (**F**), expression changes are attenuated or reversed. There are only minor differences between overall expression between P_{CKO} and C/PS_{CKO} (**G**).

H) Boxplots of composite scores showing average expression of the up- or downregulated genes from (**D-F**) at 0, 2 and 7dpc. Horizontal line = mean, box below = 25th percentile, box above = 75th percentile, grey lines = whiskers / range.

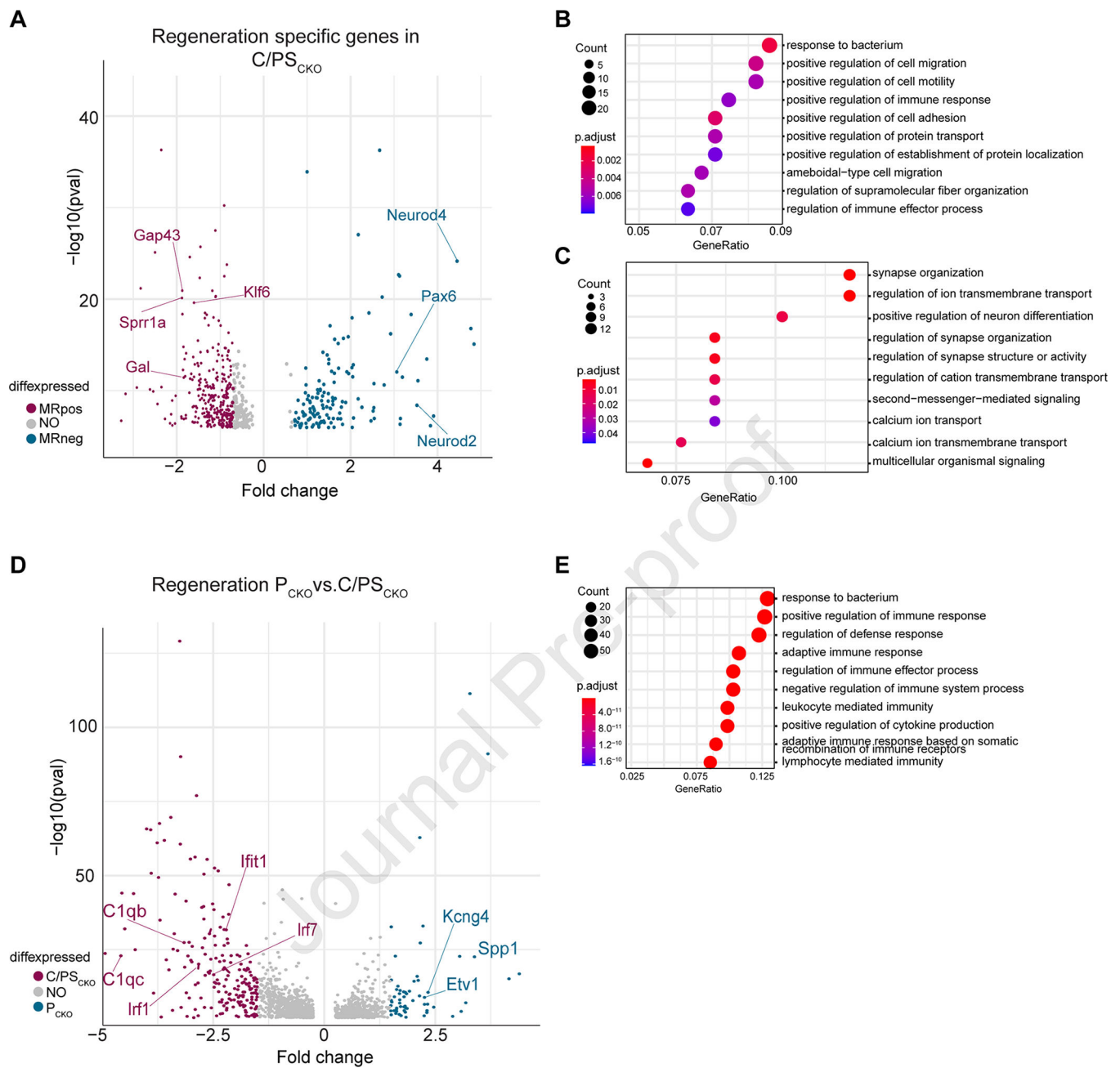


Figure 4: Gene expression analysis of regenerating RGCs

A) Volcano Plot of genes differentially expressed between MR⁺ and MR⁻ RGCs from C/PS_{CKO} retinas at 21dpc. p-value < 0.05, logFC > 0.7. Grey dots are genes not considered as highly significant DE (logFC < 0.6).

B, C) Dotplots highlighting Top10 GO-pathways enriched in regenerating (MR⁺) RGCs compared to surviving (MR⁻) RGCs (**B**) or in surviving compared to regenerating RGCs (**C**).

D) Volcano Plot of genes differentially expressed between $MR^+ P_{CKO}$ and C/PS_{CKO} RGCs. Genes associated with immune response or alphaRGCs are indicated in red and blue, respectively. Grey dots as in **(A)**.

E) Dotplot highlighting Top10 GO-pathways enriched in regenerating $MR^+ C/PS_{CKO}$ RGCs compared to $MR^+ P_{CKO}$ RGCs.

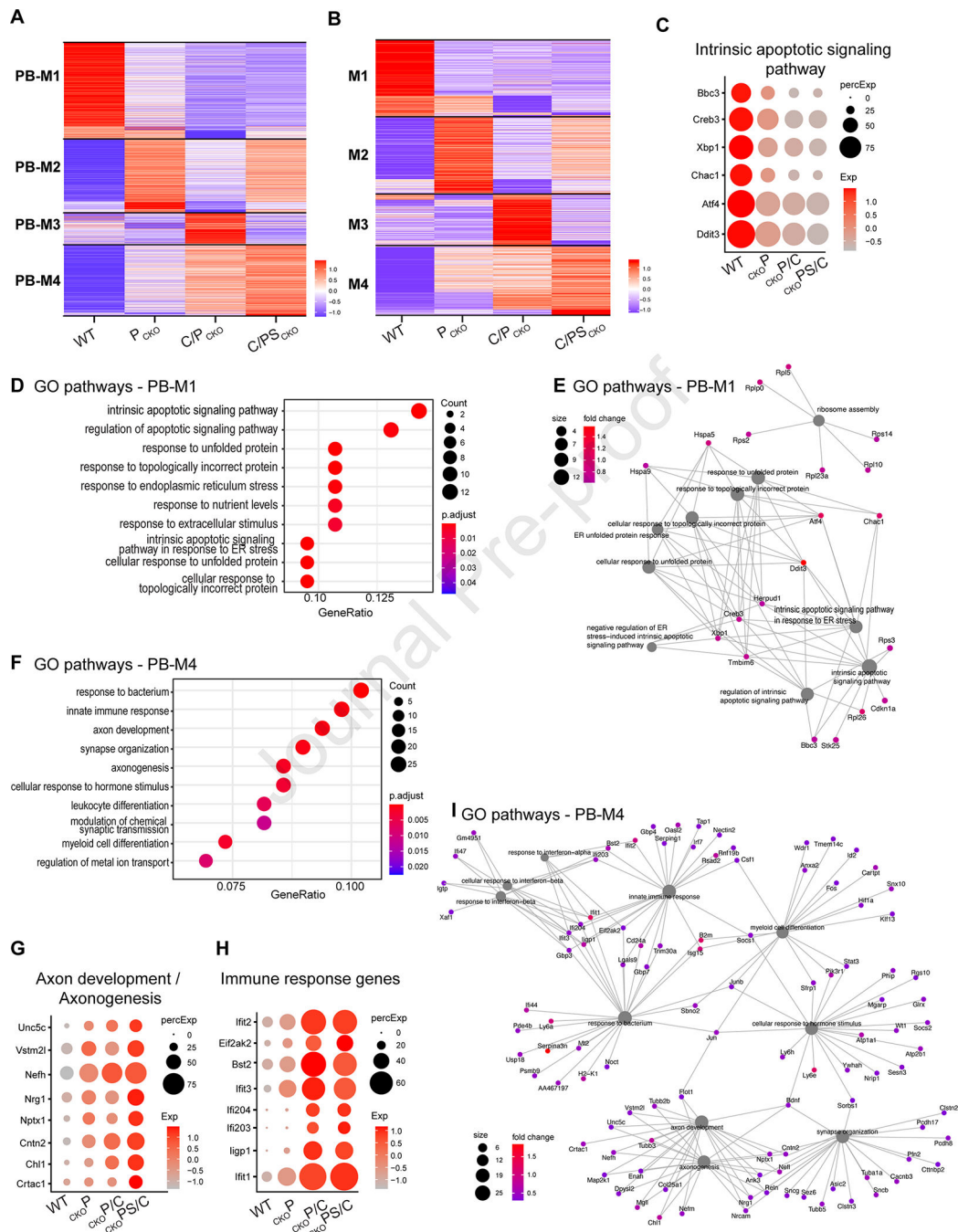


Figure 5: Gene modules revealed as genes selectively regulated by individual interventions

A,B) Heatmaps showing genes selectively expressed at 7dpc following each intervention, as calculated for each intervention against all others (**A**) or for each intervention compared to the one to its left (**B**) Expression values of each gene (row) are averaged across all RGCs in an intervention (columns) and then z-scored prior to plotting. Black bars separate genes into 4 modules (PB-M1-4).

C) Dotplot showing expression of selected apoptotic pathway associated genes from PB-M1 at 7dpc.

D,F) Top10 GO-pathways enriched in PB-M1 (**D**) or PB-M4 (**F**) ($\log_{2}FC > 0.6$, $FDR < 0.001$)

E,I) Cnet plot of Top10 pathways for PB-M1 (**E**) or PB-M4 (**I**) with associated genes. Color of dots represents the fold change of genes. Size of the grey dots refer to the number of genes enriched with the GO-term.

G,H) Dotplots showing expression of genes implicated in axonogenesis (**G**) and immune responses (**H**) from PB-M4.

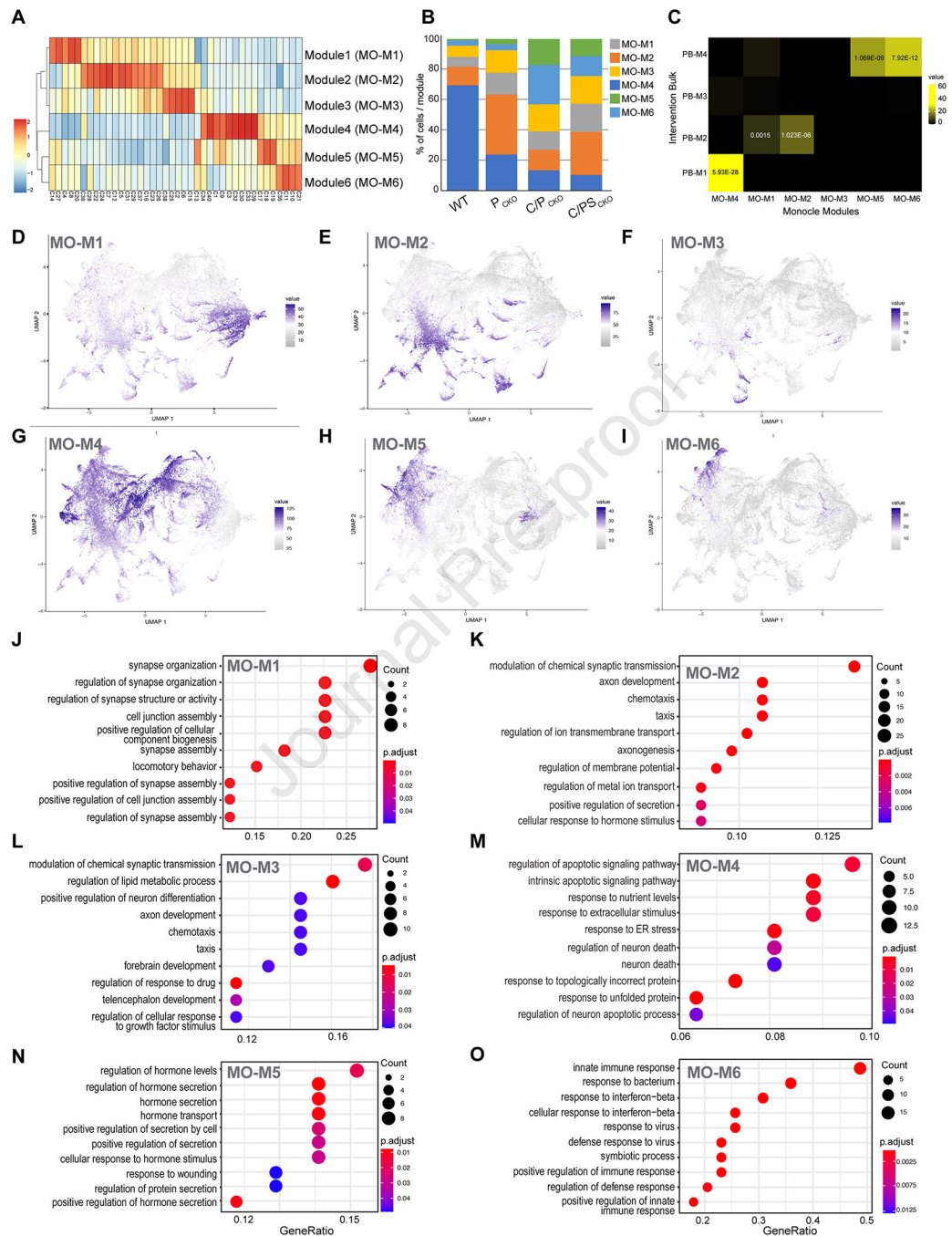


Figure 6: Gene modules revealed by single cell analysis using Monocle

A) Expression of 6 co-expression gene modules across the 40 Monocle clusters at 7dpc. Their relationships are indicated by the dendrogram to the left. Module expression is averaged across rows.

B) Proportions of RGCs belonging to sets of Monocle clusters predominantly enriched for the indicated co-expression Module in each intervention.

C) Heatmap of statistical enrichment using the hypergeometric test indicating correspondence between modules obtained from Pseudo-bulk analysis (Figure 5A) and Monocle analyses modules. Statistically significant p-values are shown.

D-I) UMAPs show enrichment co-expression Modules across RGC populations.

J-O) Top10 GO-pathways for each Monocle module. All genes contributing to the modules were considered. ($\log_{2}FC > 0.6$, $FDR < 0.001$).

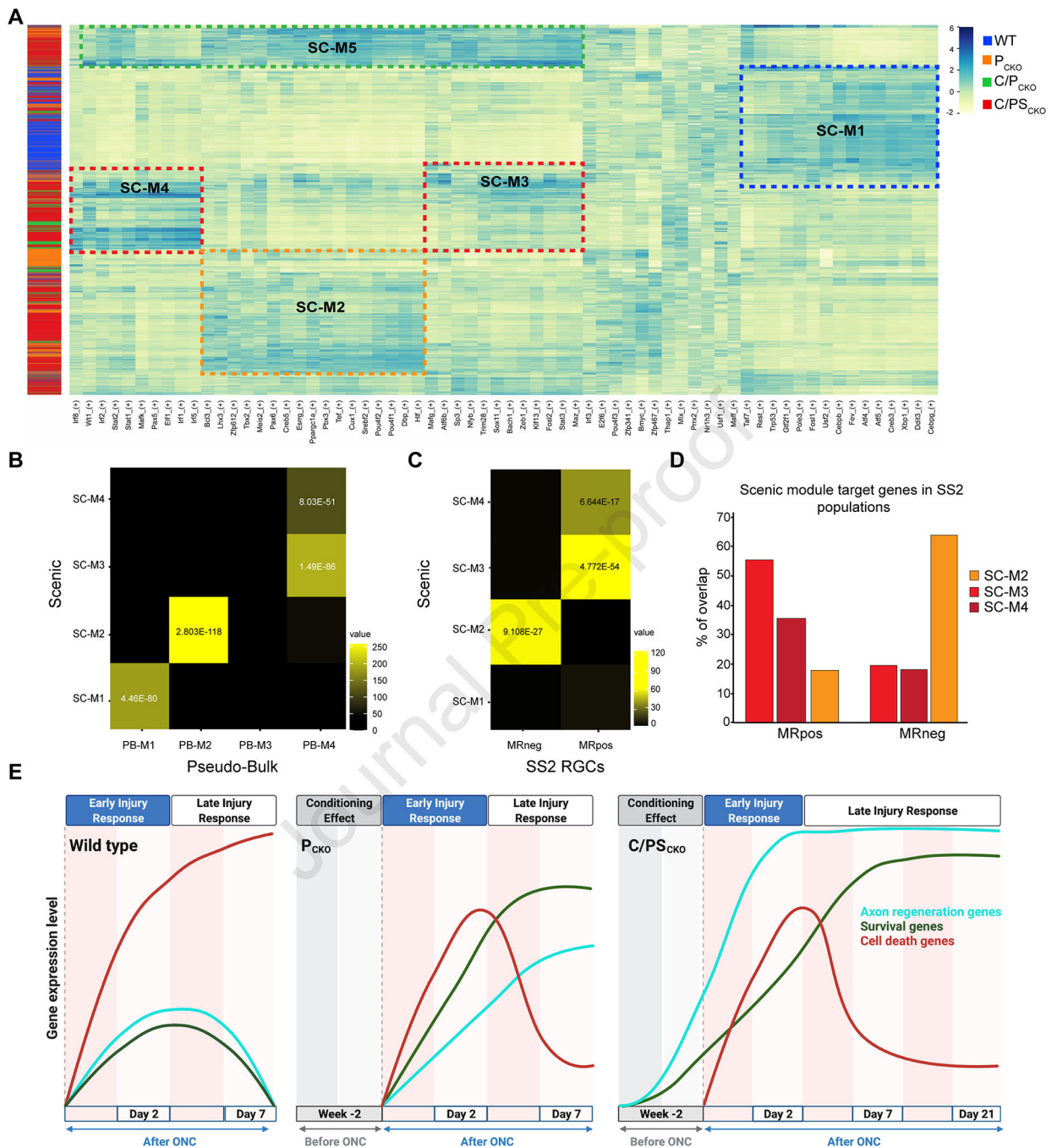


Figure 7: Gene regulatory modules revealed by Scenic

A) Heatmap of top regulon expression level (transcription factors (TF) and their putative downstream targets) in each cell at 7dpc established by Scenic analysis. Each row is a single RGC, with color bar at left indicating intervention type. Each column is a single regulon, with the TF listed at bottom. Dotted lines indicate 4 modules discussed in the text.

B,C) Heatmaps of statistical enrichment using the hypergeometric test indicating the possibility of overlap between Scenic module regulons (TFs and potential regulated target genes; y-axis) and PB-M1-4 from Pseudo-Bulk analysis (C) or genes selectively

expressed in regenerating (MR^+) or surviving (MR^-) RGCs from micro-Ruby analysis (D). Statistically significant p-values are shown.

D) Proportions of SCENIC module target genes shared with genes enriched in regenerating (MR^+) or surviving (MR^-) RGCs obtained from micro-Ruby dataset.

E) Schematic showing expression of death, survival and regeneration module genes following ONC in wild-type mice and after interventions. Data are taken from Figures 3, 7, S7 and Tran et al. (2019). However, the schematic is meant to show trends and is not quantitatively accurate. Increases prior to nerve crush reflect the “conditioning” effect of delivering interventions two weeks prior to injury, as described in the text. Created with BioRender.com

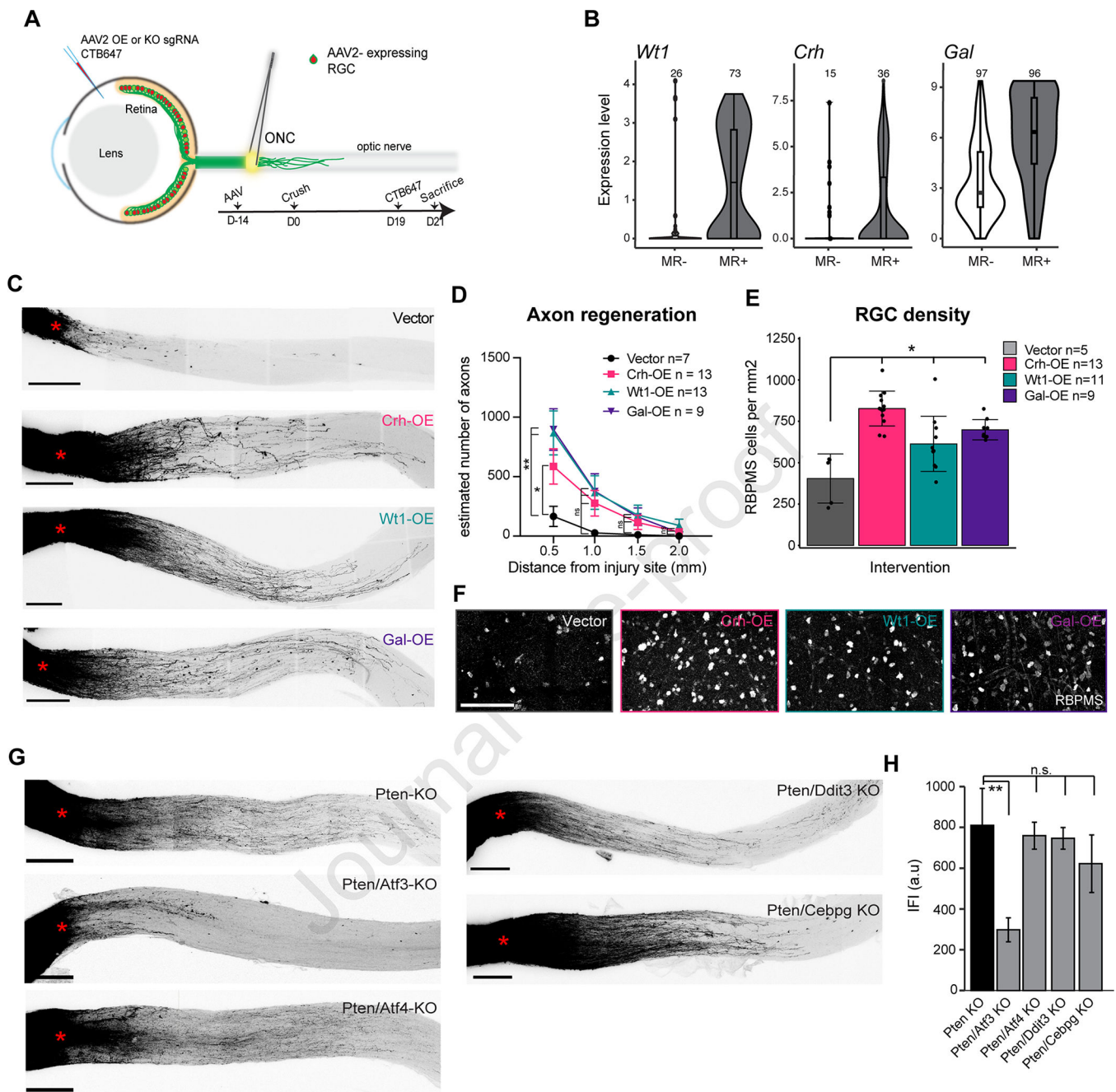


Figure 8: Genes affecting RGC axon regeneration

A) Experimental outline for *in vivo* tests of candidate regeneration-promoting genes. An AAV2 carrying a cDNA (for overexpression, OE) or sgRNA (for knockout, KO) was injected intravitreally 14 days before the crush. At 19dpc for OE or 12dpc for KO, regenerating axons were anterogradely labeled by CTB647 injection.

B) Violin plots showing expression of OE candidates in regenerating (MR⁺) and surviving (MR⁻) RGCs.

C) Maximum projections of cleared optic nerves showing anterograde-labeled RGC axons at 21dpc following indicated treatment. Scale bar = 250 μ m, red asterisks indicate crush site.

D) Quantification of axon regeneration based on images such as those in **C**. Data are shown as mean \pm SEM. p-value by Kruskal – Wallis followed by Dunn’s post hoc at each distance. $p < 0.05 = *$, $p < 0.01 = **$.

E) RGC density (RBPMS+ cells/mm²; mean \pm SD) based on images such as those in **(F)**. *adjusted p-value $<.05$ (FDR).

F) Immunohistochemistry in retinal whole mounts stained for RBPMS at 21dpc following OE-Gal, OE-Wt1 and OE-Crh. Scale bar = 100 μ m.

G) Maximum projections of cleared P_{CKO} optic nerves following indicated treatment. As in **(C)** but 14dpc.

H) Quantification of axon regeneration based on images such as those in **(G)**. Data are shown as mean \pm SEM with n = 4–6 each. ** $p < 0.01$.

KEY RESOURCES TABLE

REAGENT or RESOURCE	SOURCE	IDENTIFIER
Antibodies		
Chicken polyclonal anti-GFP	Abcam	Cat#ab13970;RRID:AB_300798
Guinea pig polyclonal anti-Rbpms	PhosphoSolutions	Cat#1832-RBPMS;RRID:AB_2492226
Mouse monoclonal anti-SMI 32	Covance	Cat#SMI-32P;RRID:AB_2314912
Rabbit monoclonal anti -Wt1	ThermoFisher	Cat#MA5-32215 RRID: AB_2809502
Rabbit polyclonal anti-Tubb3	BioLegend	Cat#802001; RRID: AB_2564645
Rabbit polyclonal anti-Cart	Phoenix Pharmaceuticals	Cat#H-003-62; RRID:H-003-62
Goat polyclonal anti- Tag-1 (Cntn2)	R&D Systems	Cat#AF4439; RRID: AB_2044647
Mouse monoclonal anti-Reelin	Abcam	Cat#ab78540; RRID:AB_1603148
Chemicals, peptides, and recombinant proteins		
Alexa-conjugated cholera toxin subunit B (CTB647)	Thermo Fisher	Cat#C34778
AMES' Medium	Sigma	Cat#A1420
Papain	Worthington	Cat#LS003126
Ovomucoid	Worthington	Cat#130042202
Fluoromount-G	Southern Biotech	Cat#0100-20
Visikol® HISTO-1™ and Visikol® HISTO-2™ Combo	Visikol	Cat#HH10
Anti-Fluorescein-POD, Fab fragments	Roche	Cat#11426346910
Anti-Digoxigenin-POD, Fab fragments	Roche	Cat#11207733910
Anti-DNP-HRP	Perkin Elmer	Cat#FP1129
TSA Cyanine 3 Plus Evaluation Kit	Perkin Elmer	Cat#NEL744E001KT (FP1170)
TSA Cyanine 5 Plus Evaluation Kit	Perkin Elmer	Cat#NEL745E001KT (FP1171)
TSA Fluorescein Plus Evaluation Kit	Perkin Elmer	Cat#NEL741E001KT (FP1168)
Dextran, Tetramethylrhodamine and Biotin, 3000MW, Lysine Fixable (micro-Ruby; MR)	Thermo Fisher	Cat#D7162
Dextran, Texas Red, 3000MW, Lysine Fixable	Thermo Fisher	Cat#D3328
Critical commercial assays		
Chromium Single Cell 3' Library & Gel Bead Kit v3, 16rxns	10X Genomics	Cat#1000075
Chromium Single Cell A Chip Kit, 16rxns	10X Genomics	Cat#1000009
Chromium i7 Multiplex Kit 96 rxns	10X Genomics	Cat#120262
In situ hybridisation (FISH) (for Atf4, Ddit3, Jam2)	Molecular Instruments	NA
Visikol® HISTO-1™ and Visikol® HISTO-2™ Combo	Visikol	Cat#HH10
Deposited data		
Gene Expression Omnibus	This manuscript	GSE202155
Experimental models: Organisms/strains		
Mouse: C57Bl/6	Charles River or Jackson Labs	Strain code #027 (CR) or JAX000664
Mouse: B6J.129S6(FVB)- <i>Slc17a6^{tm2(cre)Low}</i> /MwarJ	Jackson Labs	Cat#JAX0288663; RRID:IMSR_JAX:028863
Mouse: B6;CBA-Tg(Thy1-YFP)GJrs/GfngJ	Joshua Sanes (Feng et al., 2000; Sun et al., 2011)	Cat#JAX014130; RRID:IMSR_JAX:014130

REAGENT or RESOURCE	SOURCE	IDENTIFIER
Mouse: B6;129- <i>Gt(ROSA)26Sor^{tm1(CAG-cas9*,-EGFP)Fz}hJ</i>	Jackson Labs	Cat#JAX024857; RRID:IMSR_JAX:024857
Mouse: B6.129S4- <i>Pten^{flHwu}/J</i>	Jackson Labs	Cat#JAX006440; RRID:IMSR_JAX:006440
Mouse: B6;129S4- <i>Socs3^{tm1Ayo}/J</i>	Jackson Labs	Cat#JAX010944; RRID:IMSR_JAX:010944
Oligonucleotides		
Primer used to generate ISH probes	IDT	Table S8
Primer for overexpression cloning	IDT	Table S8
Primer for sgRNA cloning	IDT	Table S8
Recombinant DNA		
pAAV2-hSyn-hChr2(H134R)-EYFP	Gift from Karl Deisseroth	Addgene plasmid Cat#26793; RRID:Addgene_26973
AAV-U6-sgRNA-hSyn-mCherry	Gift from Alex Hewitt	Addgene plasmid Cat#87916; RRID:Addgene_87916
pAAV2-CAG-Cre-WPRE-hGH	BCH Viral Core	Belin et al.,2015
pAAV2-hSyn-Gal-WPRE	BCH Viral Core	NA
pAAV2-hSyn-Crh-WPRE	BCH Viral Core	NA
pAAV2-hSyn-Wt1-WPRE	BCH Viral Core	NA
pAAV2-hSyn-CNTF-WPRE	BCH Viral Core	NA
Software and algorithms		
ImageJ (Fiji)	(Schindelin et al., 2012)	https://imagej.net/Fiji
Cell Profiler	(Carpenter et al., 2006)	https://cellprofiler.org
Prism 8.0	GraphPad Software	https://www.graphpad.com/
Cell Ranger v3.1.0	10X Genomics	https://support.10xgenomics.com/single-cell-gene-expression/software/downloads/latest
R for statistical computing version 4.0.2	N/A	https://cran.r-project.org/
Bioconductor software packages	(Gentleman et al., 2004)	http://bioconductor.org/
Python version 3.6.13	Python Software Foundation	https://www.python.org/
Anaconda version 4.3.30	2017 Continuum Analytics, Inc	https://docs.conda.io/en/latest/
Matlab Mathworks	custom script	https://www.mathworks.com/
Other		
LSM 710 scanning confocal microscope	Zeiss	N/A
Olympus FV-1000 confocal microscope	Olympus	N/A
HiSeq 2500 System	Illumina	N/A
NextSeq 500 System	Illumina	N/A
Nova Seq	Illumina	N/A
Chromium controller	10x Genomics	N/A
MoFlow Astrios FACS sorter	Beckman Coulter	N/A
Biomek Span-8	Beckman Coulter	N/A